LIESOLVER*: A PDE-constrained solver for IBVPs using Lie symmetries

René P. Klausen^{a,†,§}, Ivan Timofeev^{a,†}, Johannes Frank^a, Jonas Naujoks^a, Thomas Wiegand^{a,b,c}, Sebastian Lapuschkin^{a,d}, and Wojciech Samek^{a,b,c}

a Department of Artificial Intelligence, Fraunhofer Heinrich Hertz Institute
 b Department of Electrical Engineering and Computer Science, Technische Universität Berlin
 c BIFOLD - Berlin Institute for the Foundations of Learning and Data
 d Centre of eXplainable Artificial Intelligence, Technological University Dublin

† Equal contribution § Corresponding author rene.pascal.klausen@hhi.fraunhofer.de

Abstract

We introduce a method for efficiently solving initial-boundary value problems (IBVPs) that uses Lie symmetries to enforce the associated partial differential equation (PDE) exactly by construction. By leveraging symmetry transformations, the model inherently incorporates the physical laws and learns solutions from initial and boundary data. As a result, the loss directly measures the model's accuracy, leading to improved convergence. Moreover, for well-posed IBVPs, our method enables rigorous error estimation. The approach yields compact models, facilitating an efficient optimization. We implement LIESOLVER and demonstrate its application to linear homogeneous PDEs with a range of initial conditions, showing that it is faster and more accurate than physics-informed neural networks (PINNs). Overall, our method improves both computational efficiency and the reliability of predictions for PDE-constrained problems.

Keywords: Physics-Informed Machine Learning, Physics-Informed Neural Networks, Scientific Machine Learning, Lie Symmetries, Partial Differential Equations, Initial-Boundary Value Problems

1 Introduction

Partial differential equations (PDEs) appear in nearly every scientific discipline, from fluid dynamics to quantitative finance. This ubiquity makes the development of reliable and efficient PDE solvers a central challenge in the field of computational science. In particular, the goal is to find specific solutions of PDEs that satisfy additional initial and/or boundary conditions; this setting is commonly referred to as the initial-boundary value problem (IBVP). While classical numerical methods, such as finite difference and finite element techniques [21], can effectively address these

^{*}In German, "Lies" is the imperative of "lesen" ("read"); "LieSolver" playfully suggests "Lies Olver"— to read Olver. We use Olver's book [31] as our primary source on Lie symmetries, prolongation, and symmetry-generated solution transformations.

problems, their computational cost increases dramatically with the dimensionality of the problem. In particular, most classical methods require a domain discretization, which allows the evaluation of the function at a finite set of predetermined grid points only. As a result, high-dimensional PDEs present particularly daunting challenges that necessitate innovative solution strategies as outlined in [17].

To this end, various approaches have been developed that employ machine learning techniques to tackle these problems. Early approaches to solving differential equations with neural networks date back to the pioneering work by Lagaris et al.[19], who proposed feedforward architectures that satisfy boundary and initial conditions by construction. Furthermore, various machine learning techniques have been explored to address these challenges, such as the work by [38], which aims to recover analytical closed-form solutions through genetic programming.

The introduction of physics-informed neural networks (PINNs) [32] in 2017 revitalized interest in the field of physics-informed machine learning and the application of machine learning-based techniques for solving PDEs. Similar to the Deep Galerkin Method [35], PINNs utilize multiple loss terms corresponding to the PDE and the boundary and/or initial conditions to approximate solutions by minimizing the loss. Hence, the network is guided – but not guaranteed – to respect the physics. These methods have demonstrated notable success across various applications, by no means limited to physics, in solving IBVPs [17]. A large body of follow-up work has sought to improve training stability and scalability using a plethora of approaches, including domain decomposition [15], adaptive loss balancing [42], improved optimizers [33, 39], resampling [20, 25, 44] and multifidelity extensions [23]. Although promising, PINNs often suffer from unstable convergence [18, 41]. In practice, networks can reach very small PDE residuals while failing to approximate the true solution well. The reason is that the PDE loss term used in PINNs is not monotone with respect to the solution error. As a result, the training loss does not necessarily provide predictive power: low loss does not automatically imply high accuracy. This issue limits the reliability of PINNs as general-purpose PDE solvers. Despite numerous enhancements for PINNs, the aforementioned issue is inherent to the intrinsic structure of PINNs and their underlying optimization scheme.

In general, there are several ways to incorporate physics into a machine learning model: (a) by informing the data, (b) through the loss function, or (c) by modifying the model's architecture [17]. Whereas classical PINNs inform the model solely through the loss function (b), there are also hybrid approaches, such as hard-constraint PINNs [22], which utilize a PDE-informed loss function in conjunction with a boundary-conditions-informed architecture. In addition, there are several approaches where physics is baked directly into the model architecture. Examples include convolutional networks that hard-code translation symmetry [8], equivariant networks for three-dimensional particle systems [37], and structure-preserving models such as Hamiltonian [13] or Lagrangian neural networks [9]. These architectures ensure physical consistency by design, but are usually specialized to certain physical aspects.

In the realm of physics, symmetries play a dominant role [43], inspiring diverse machine learning approaches which are "symmetry-informed". Examples include symmetry-informed data augmentation for neural PDE solvers [5], self-supervised pretraining based on Lie symmetry transformations [24], and symmetry-regularized PINNs [1], which all exploit the invariance structure of the underlying equations to improve generalization and sample efficiency. Similarly, [47] leverages Lie symmetry groups to generate data for supervised learning, providing an alternative to physics-

informed training. Other methods embed invariant surface conditions into the loss [48] to enhance the PINN method. Yet another recent line of work [45, 46] utilizes Lie symmetries to discover them from data and integrate them into learning architectures, improving long-term predictive accuracy and facilitating practical applications such as equation discovery.

In our approach, we leverage the inherent symmetries of PDEs, namely their Lie symmetries, by integrating them directly into the model structure. This method is in principle possible for any PDE or any corresponding Lie symmetry, as these symmetries inherently generate parametrized and expressive solutions by themselves. Our work integrates predetermined parametrized Lie symmetries as learnable building blocks, enabling the model to compose symmetry transformations to solve PDEs while provably remaining in the space of solutions of the underlying PDE. Consequently, for every set of model parameters, the resulting model exactly satisfies the PDE. As a result, the optimization problem reduces to fitting the initial-boundary values only. This makes the optimization significantly more controllable and eliminates the need for difficult-to-handle PDE loss term used in PINNs, which in our opinion represents the greatest challenge in the PINN method.

Consequently, in our model, a decrease of the loss function directly corresponds to an enhancement of the accuracy of the prediction. Hence, in contrast to PINNs, the loss function serves as a reliable metric for evaluating training progress. In addition, for well-posed IBVPs, one can derive rigorous error bounds that scale with the test loss. Moreover, this approach allows us to design significantly smaller models (in terms of the number of parameters), while preserving a high degree of expressiveness. As a result, this enables more robust optimization leading to more accurate approximations in significantly less time compared to PINNs.

The article is structured as follows: We begin by introducing the underlying problem: IBVPs (section 2.2) with their associated PDEs (section 2.1). These concepts are introduced in a way that is useful for the study of Lie symmetries, which are reviewed in section 2.3. We complement the discussion of Lie symmetries with more details in appendix A.1. In section 3 we propose our new method LieSolver, which is specialized to linear homogeneous PDEs. section 4 presents our experiments, testing the scope of LieSolver and comparing it with PINNs, demonstrating that our approach leads to more accurate solutions that can be computed significantly faster.

To summarize the contributions of our work, we provide:

- The new machine learning framework LIESOLVER based on Lie symmetries, which aims to solve IBVPs. This method will enforce PDE exactly, by the use of a PDE-informed architecture. Learning happens only on the boundary domain and requires no data, as arbitrary data points can be sampled as needed. Our approach is currently limited to linear homogeneous PDEs.
- An illustration of how to derive rigorous error bounds from the test loss in well-posed problems.
- The path towards theoretical convergence guarantees. We do not prove any bounds rigorously.
- Benchmark experiments demonstrating higher solution accuracy and faster compute times compared to vanilla PINNs.
- An improved interpretability through access to a symbolic decomposition of the solution.

2 Theoretical Background

The main focus of this article is to solve initial-boundary-value problems (IBVPs) effectively by using machine learning techniques. We will introduce IBVPs in section 2.2 along with their associated partial differential equations (PDEs) (section 2.1), while placing a particular emphasis on their symmetries in section 2.3. For readers seeking a quick overview, we recommend focusing on section 2.3. A more comprehensive description of the topics discussed will be compiled in appendix A.1. For a detailed exploration of these subjects, we refer to [31] as an extensive standard source, [2, 3, 30] for alternative presentations, [10] for a focus on Lie groups, and [27] for an overview, including a historical perspective.

2.1 Partial Differential Equations (PDEs)

In a nutshell, PDEs are just equations containing derivatives. When studying symmetries of PDEs, it is often convenient to think of their solutions as parametrized surfaces, instead of functions, which enables a geometric treatment. In the following, we develop this idea rigorously and introduce the key concepts. This summary is oriented towards the description in [31]. For a more general perspective on PDEs we recommend [11, 16, 29, 34].

Consider n independent variables $x = (x_1, \ldots, x_n) \in X = \mathbb{R}^n$ and m dependent variables $u = (u^1, \ldots, u^m) \in \mathcal{U} = \mathbb{R}^m$. This terminology reflects that we will later treat solutions as maps from X to \mathcal{U} . In addition to the dependent and independent variables, the PDE also contains derivatives. Therefore, we denote by $d \in \mathbb{N}$ the order of the considered PDE, i.e., the order of its highest derivative. For n independent variables, the number of distinct partial derivatives up to order d is given by $\binom{n+d}{d}$. We prolong the space \mathcal{U} to include all partial derivatives up to order d, which we denote by $\mathcal{U}^{(d)} := \mathbb{R}^{m \binom{n+d}{d}}$. By these definitions, a system of p PDEs of order d is given as a set of equations

$$\mathcal{D}_j(x, u^{(d)}) = 0, \qquad j = 1, \dots, p \tag{1}$$

where we assume $\mathcal{D}: X \times \mathcal{U}^{(d)} \to \mathbb{R}^p$ to be smooth. Accordingly, we describe PDEs as functions of the independent variables and the prolonged dependent variables.

In order to connect the placeholder variable $u^{(d)}$ to the actual derivatives, we introduce the prolongation of functions. For a sufficiently smooth function $f: \Omega \to \mathcal{U}$ with $\Omega \subseteq X$ open, its d-th prolongation $\operatorname{pr}^{(d)} f: \Omega \to \mathcal{U}^{(d)}$ is defined as the tuple

$$\operatorname{pr}^{(d)} f(x) := \left(\partial_J f(x) \right)_{J \in [n]^d} \in \mathcal{U}^{(d)} , \qquad (2)$$

where $[n]^d := \{ \sigma \subseteq \{1, ..., n\} : |\sigma| \leq d \}$ contains all subsets of [n] with at most d elements (including the empty set), and we write for a set $J = \{j_1, ..., j_k\}$

$$\partial_j := \frac{\partial}{\partial x_j}, \qquad \partial_{\{j_1, \dots, j_k\}} := \partial_{j_1} \dots \partial_{j_k} \quad \text{and} \quad \partial_{\emptyset} f := f$$
 (3)

¹We will always assume smooth functions, such that derivatives will commute. The number of partial derivatives follows from the combinatorial identity $\sum_{i=0}^{d} \binom{n+i-1}{i} = \binom{n+d}{d}$ for $d \ge 0$ and n > 0, which can be easily shown by induction.

for brevity. Thus, the prolongation explicitly lists all derivatives up to order d. For instance, for a function $f: \mathbb{R}^2 \to \mathbb{R}$ we get $\operatorname{pr}^{(2)} f(x,y) = (f, f_x, f_y, f_{xx}, f_{xy}, f_{yy}) \in \mathcal{U}^{(2)} \cong \mathbb{R}^6$.

A sufficiently smooth function $f: \Omega \to \mathcal{U}$, with $\Omega \subseteq X$ open, is called a solution of the PDE system \mathcal{D} if

$$\mathcal{D}(x, \operatorname{pr}^{(d)} f(x)) = 0 \qquad \forall x \in \Omega . \tag{4}$$

It is important to note, that there is no general theory to find solutions of PDEs. However, for the further treatment, it is useful to classify PDEs with respect to their properties. We call a PDE (system) \mathcal{D} linear if we can write it in the form

$$\mathcal{D}(x, \operatorname{pr}^{(d)} f(x)) = h(x) + \sum_{J \in [n]^d} a_J(x) \partial_J f(x)$$
(5)

for some functions $h, a_J : X \to \mathbb{R}^p$. If in addition $h(x) \equiv 0$, we call the PDE (system) linear homogeneous. For any linear homogeneous PDEs, we have that if f_1 and f_2 are two solutions of the PDE, then so is $\alpha f_1 + \beta f_2$ for any $\alpha, \beta \in \mathbb{R}$. In particular, it holds that $f(x) \equiv 0$ is always a solution for any linear homogeneous PDE. If a linear homogeneous PDE does not contain a term depending on u, it additionally is true that every constant function solves this PDE.

2.2 Initial-boundary value problems (IBVPs)

Since PDEs usually admit infinitely many solutions, we impose additional constraints in the form of *initial-boundary conditions* (IBC) to ensure uniqueness. To simplify the notation, we will not explicitly distinguish between time and spatial coordinates. Hence, initial and boundary conditions get the same form. Let $\Omega \subset X$ be a bounded domain, where its boundary $\partial\Omega$ contains smooth, connected components $\Gamma_1, \ldots, \Gamma_r \subseteq \partial\Omega$. For each Γ_k , we introduce a condition of the form

$$\mathcal{B}_k(x, u, u_n) = 0 \quad \text{for all } x \in \Gamma_k$$
 (6)

with $\mathcal{B}_k : \Gamma_k \times \mathcal{U} \times \mathcal{U} \to \mathbb{R}$. The symbol u_n is a placeholder, which will later be associated with the normal derivative. A PDE system \mathcal{D} together with associated IBCs $\mathcal{B}_1, \ldots, \mathcal{B}_r$ defines an *initial-boundary value problem* (IBVP). A sufficiently smooth function $f : \overline{\Omega} \to \mathcal{U}$ is called a *solution of the IBVP* if

$$\mathcal{D}(x, \operatorname{pr}^{(d)} f(x)) = 0 \qquad \forall x \in \Omega$$
 (7)

$$\mathcal{B}_k\left(x, f(x), \frac{\mathrm{d}f}{\mathrm{d}\boldsymbol{n}}(x)\right) = 0 \qquad \forall x \in \Gamma_k, \ k = 1, \dots, r \ ,$$
 (8)

where $\frac{\mathrm{d}f}{\mathrm{d}\mathbf{n}}(x) = \nabla f(x) \cdot \hat{n}(x)$ is the normal outward derivative on Γ_k .

In the following, we will always focus on well-posed IBVPs, meaning that (i) the IBVP has a solution, (ii) the solution is unique, and (iii) the solution depends continuously on the prescribed initial and boundary data. The precise definition of these three properties depends on the specific problem being considered, and there is no commonly agreed definition, as noted in [16]. Typically, we restrict the space of possible solutions to smooth functions and may add further restrictions, e.g., certain assumptions on the growth at infinity, in order to specify uniqueness. To illustrate the last condition in practice, we give the following example.

Example 2.1 [heat equation and reverse heat equation]: Consider the two IBVPs of the so-called reverse heat equation in the domain $x \in [0, 2\pi)$, t > 0 with

$$u_t + u_{xx} = 0, \ u(x,0) = 0, \ u(0,t) = u(2\pi,t) = 0$$
 (9)

$$v_t + v_{xx} = 0, \ v(x,0) = \epsilon \sin(x), \ v(0,t) = v(2\pi,t) = 0$$
 (10)

with $\epsilon > 0$. It is not hard to verify the two solutions $u(x,t) \equiv 0$ and $v(x,t) = \epsilon \sin(x)e^t$. These two problems only differ in the initial condition, having the distance $||u(0) - v(0)||_{\infty} = \epsilon$, with the norm $||f(t)||_{\infty} := \max_{x \in [0,2\pi)} |f(x,t)|$. Hence, the initial conditions are arbitrary close for small ϵ . However, the distance between solutions is given by $||u(t) - v(t)||_{\infty} = \epsilon e^t$, which is not bounded on the domain. Hence, the solution will not depend continuously on the initial data, and this problem is ill-posed.

In comparison, consider a slightly modified version of the problem (heat equation)

$$u_t - u_{xx} = 0, \ u(x,0) = 0, \ u(0,t) = u(2\pi,t) = 0$$
 (11)

$$v_t - v_{xx} = 0, \ v(x,0) = \epsilon \sin(x), \ v(0,t) = v(2\pi,t) = 0$$
 (12)

which results in the solutions $u(x,t) \equiv 0$ and $v(x,t) = \epsilon \sin(x)e^{-t}$. In that case, the distance between the solutions is given by $||u(t) - v(t)||_{\infty} = \epsilon e^{-t} \le \epsilon$. Hence, the map from initial data to solutions is (locally) Lipschitz continuous

$$\|u(t) - v(t)\|_{\infty} \le C \|u(0) - v(0)\|_{\infty} \tag{13}$$

with Lipschitz constant C=1. Hence, we confirmed the well-posedness of the heat equation with Dirichlet conditions.

2.3 Lie Symmetries

PDEs can be invariant under certain symmetries, and so their set of solutions has to respect the same symmetries. Let us illustrate this behaviour on the differential equation $u_{xx} = 0$. Obviously, if u = f(x) is a solution, then so is $u = f(x) + \vartheta$, as well as $u = e^{\vartheta} f(x)$ for any $\vartheta \in \mathbb{R}$. Hence, the underlying PDE comes with a translation and scaling invariance

$$T^1_{\vartheta}: f(x) \mapsto f(x) + \vartheta \quad \text{and} \quad T^2_{\vartheta}: f(x) \mapsto e^{\vartheta} f(x) \quad .$$
 (14)

Moreover, these symmetry transformations will generate a group structure, i.e., we have a neutral element $T_0^i = e$, inversions $\left(T_\vartheta^i\right)^{-1} = T_{-\vartheta}^i$ and $T_{\vartheta_1}^i \circ T_{\vartheta_2}^i = T_{\vartheta_1+\vartheta_2}^i$. Thus, we obtain a two-dimensional group, which is spanned by two one-parameter groups.

The rigorous study of these symmetry groups naturally leads to the framework of *Lie groups* [10], which provide the mathematical structure for continuous transformation groups. A Lie group is a smooth, finite-dimensional manifold endowed with a group structure² such that both the multiplication and inversion maps are smooth.

Symmetry transformations can be described as actions of the Lie groups on manifolds. For a Lie group G and a smooth manifold M, this action $\circ: G \times M \to M$ is required to be compatible

²A group (G, \cdot) is a set G equipped with a binary operation $\cdot : G \times G \to G$ that is associative, has a unique identity element $e \in G$, and assigns to each $g \in G$ a unique inverse g^{-1} .

with the group axioms, i.e., we demand $g_1 \circ (g_2 \circ x) = (g_1 \cdot g_2) \circ x$ and $e \circ x = x$ for any $g_1, g_2 \in G$ and all $x \in M$.

Depending on the group G and the manifold M, not all of these actions may be defined, which is why we allow restricting these actions to a subset $\mathscr{U} \subseteq G \times M$ containing the identity $\{e\} \times M \subseteq \mathscr{U}$. We will call this restriction a *local group of transformations*. Note that this restriction to group elements around the identity do not pose any serious limitations, since every element of the full Lie group G can be written as a finite product of elements which are close to the identity (compare [31, thm. 1.22 and prop. 1.24]).

In order to connect a PDE solution to a manifold, let $f: \Omega \to \mathcal{U}$ be a sufficiently smooth function with $\Omega \subseteq X$. Its graph is defined as

$$\Gamma_f := \{ (x, f(x)) \mid x \in \Omega \} \subseteq \Omega \times \mathcal{U} , \qquad (15)$$

a smooth submanifold of $X \times \mathcal{U}$. If G is a (local) group of transformations acting on $X \times \mathcal{U}$, then for $g \in G$ we define the transformed graph as

$$g \circ \Gamma_f := \{ (\tilde{x}, \tilde{u}) = g \circ (x, u) \mid (x, u) \in \Gamma_f \} . \tag{16}$$

In the case where we can write the transformed graph $g \circ \Gamma_f = \Gamma_{\tilde{f}}$ as a graph of another function \tilde{f} , we simply write $\tilde{f} = g \circ f$. Note that for elements g close to the identity, we always find a (single-valued) function \tilde{f} with that property.

A symmetry group of a PDE \mathcal{D} is a local group of transformations G acting on $M \subseteq X \times \mathcal{U}^{(d)}$, such that whenever u = f(x) is a solution of \mathcal{D} , and $g \circ f$ is defined for $g \in G$, then $u = g \circ f(x)$ will be a solution of \mathcal{D} as well.

To illustrate these concepts, we discuss the symmetry group of the 1-dimensional heat equation. We will provide a discussion on how to actually compute these symmetry groups in examples A.2 to A.4.

Example 2.2 [1-dimensional heat equation]: Consider the heat equation

$$\mathcal{D}(x, t, u^{(2)}) = u_t - u_{xx} \tag{17}$$

where n = 2, d = 2, m = 1 and p = 1. It admits the following six one-parameter symmetry transformations [31]:

$$T^1_{\vartheta}: f(x,t) \mapsto f(x-\vartheta,t)$$
 (18)

$$T_{\vartheta}^2: f(x,t) \mapsto f(x,t-\vartheta),$$
 (19)

$$T_{\vartheta}^3: f(x,t) \mapsto e^{\vartheta} f(x,t)$$
 (20)

$$T_{\vartheta}^{4}: f(x,t) \mapsto f(e^{-\vartheta}x, e^{-2\vartheta}t) \tag{21}$$

$$T_{\vartheta}^{5}: f(x,t) \mapsto e^{-\vartheta x + \vartheta^{2}t} f(x - 2\vartheta t, t)$$
 (22)

$$T_{\vartheta}^{6}: f(x,t) \mapsto \frac{1}{\sqrt{1+4\vartheta t}} \exp\left(\frac{-\vartheta x^{2}}{1+4\vartheta t}\right) f\left(\frac{x}{1+4\vartheta t}, \frac{t}{1+4\vartheta t}\right)$$
(23)

for any $\vartheta \in \Theta \subseteq \mathbb{R}$. Note that, we can use different values ϑ for any of these transformations, and that – depending on the domain Ω of f – we may rescrict the domain for T^6 to $\Theta \subseteq \mathbb{R}$, to avoid

singularities. In addition, there is an additional symmetry transformation, reflecting the linearity, i.e., for any solution $\alpha(x,t)$ of (17), we have the symmetry

$$T_{\vartheta}^{\alpha}: f(x,t) \mapsto f(x,t) + \vartheta \alpha(x,t)$$
 (24)

Hence, for any solution u = f(x,t) of the heat equation (17), applying any of the aforementioned transformations produces another possible solution. As an example, for the constant solution $f(x,t) \equiv 1$ and after applying the transformation T_{ϑ}^6 , obtains the function $u = \frac{1}{\sqrt{1+4\vartheta t}} \exp\left(\frac{-\vartheta x^2}{1+4\vartheta t}\right)$ that also solves the heat equation, whenever this function is defined, i.e. for $1+4\vartheta t \neq 0$.

While the transformations T^1, \ldots, T^4 in example 2.2 can be found by carefully observing the differential equation (17), T^5 and T^6 are far from being trivial to be obtained by reading the PDE. However, there exists a concrete recipe for how to compute these transformations, which we will summarize in appendix A.1. There are also plenty of implementations for the computation of Lie symmetries, and we refer to [28] for a current approach, and [6, 7, 14, 36] for an overview about different implementations.

3 LieSolver

In this section, we introduce LIESOLVER, a solver for IBVPs of linear homogeneous PDEs that enforces the PDE exactly by construction. The model is a linear combination of functions generated by parameterized Lie-symmetry transformations. Since each term satisfies the PDE, optimization reduces to fitting initial and boundary conditions. We formalize this construction and the IBC loss in section 3.1, and outline the optimization algorithm, which includes greedy term selection, variable projection for linear coefficients, and nonlinear least squares for transformation parameters, in section 3.2.

3.1 Basic structure & motivation behind LieSolver

Let $\mathcal{D}(x, u^{(d)}) = 0$ denote a linear homogeneous PDE and let $f: \Omega \to \mathcal{U}$ be a solution of this PDE. As discussed in section 2.3, a Lie symmetry T_{ϑ} of \mathcal{D} is a smooth, invertible transformation, parametrized by $\vartheta \in \Theta \subseteq \mathbb{R}$, with the property that transforming the solution with T_{ϑ} yields another solution of the PDE \mathcal{D} . In particular, as noted in section 2.1 any linear homogeneous PDE will have the following symmetry:

$$T_{\vartheta}^{\alpha}: f(x) \mapsto f(x) + \vartheta \ \alpha(x) \ ,$$
 (25)

where $x \in X$, $\vartheta \in \mathbb{R}$ and $\alpha : \Omega \to \mathcal{U}$ is an arbitrary solution of the PDE. In different terms, for any linear homogeneous PDE, the linear combination of solutions is a solution as well, which is also known as the superposition principle.

Since Lie symmetries form a group, concatenating different Lie symmetries yields another valid Lie symmetry. Thus, given a solution, one can generate a family of new solutions by successive applications of these transformations. Finding an initial solution is often straightforward. For instance, any linear homogeneous PDE admits the trivial $f(x) \equiv 0$ solution. In addition, a constant function solves every linear homogeneous PDE without a term containing u, e.g. $f(x) \equiv 1$ is a solution for heat equation, Laplace equation and wave equation. We refer to such solutions as seed solutions, denoted f_{seed} , and they are typically easy to obtain for a given PDE.

Hence, when starting with one or several seed solutions and applying various Lie transformations, the resulting functions will still constitute exact solutions of the PDE. This reveals a remarkable fact: a single seed solution, together with the action of a Lie group, can define expressive solution (sub)spaces via superposition. We illustrate this in the following example.

Example 3.1: Consider the following seed solution of the heat equation (17):

$$f_{\text{seed}}(x,t) = \sin(x) e^{-t} . \tag{26}$$

Applying the transformation T_{ϑ}^4 from example 2.2 with $\vartheta = -\ln \lambda$, one obtains the family of solution $\sin(\lambda x)e^{-\lambda^2 t}$ for any $\lambda > 0$.

It is a well-known result [4, sec. 10.5] that the IBVP for the heat equation $u_t = u_{xx}$ on (0,L) with u(0,t) = u(L,t) = 0 and $u(x,0) = \sum_{n=1}^{\infty} a_n \sin(n\pi x/L)$ admits the unique solution $u(x,t) = \sum_{n=1}^{\infty} a_n \sin(n\pi x/L) e^{-(n\pi/L)^2 t}$. Hence, even with one specific Lie transformation, we can approximate a certain type of IBVP arbitrary well.

Thus, by applying a sequence of Lie symmetries T^l to a given f_{seed} , we obtain an expressive function

$$f(x; \vartheta_1, \dots, \vartheta_k) = T_{\vartheta_k}^{l_k} \circ \dots \circ T_{\vartheta_1}^{l_1} \circ f_{\text{seed}}(x) , \qquad (27)$$

that remains a solution of the underlying PDE \mathcal{D} for any value of $\boldsymbol{\vartheta} = (\vartheta_1, \dots, \vartheta_k) \in \mathbb{R}^k$, whenever the composed function is defined.

In the approach of LIESOLVER, we consider a set $S = \{f^1(x; \boldsymbol{\vartheta}^1), \dots, f^N(x; \boldsymbol{\vartheta}^N)\}$ of expressive functions, where each function f^i is constructed from one or several seed solutions in the form of (27). We refer to these functions as *base solutions*³. We will discuss in section 3.2 more in detail, how to choose "good" base solutions for a given problem.

The central idea of LieSolver is to choose certain base solution and combine them linearly. In this procedure we can also use the same base solution several times with different parameters, i.e.

$$f_{LS}(x; a_1, \dots, a_M, \boldsymbol{\vartheta}_1^{j_1}, \dots, \boldsymbol{\vartheta}_M^{j_M}) = \sum_{i=1}^M a_i f_i^{j_i}(x; \boldsymbol{\vartheta}_i^{j_i}) ,$$
 (28)

which constitutes a very expressive function covering a major part of the solution space of the PDE. When the parameters $\boldsymbol{\vartheta}_{i}^{j_{i}}$ are specified to certain values $\hat{\boldsymbol{\vartheta}}_{i}^{j_{i}}$, we will call the collection of base solutions appearing in (28) the active set $\mathcal{A} = \{f_{1}^{j_{1}}(x; \hat{\boldsymbol{\vartheta}}_{1}^{j_{1}}), \dots, f_{M}^{j_{M}}(x; \hat{\boldsymbol{\vartheta}}_{M}^{j_{M}})\}$. Note that each $\boldsymbol{\vartheta}_{i}^{j_{i}}$ may possibly consist of several parameters as given in (27). To shorten the notation, we write $\boldsymbol{\theta} = (\boldsymbol{\vartheta}_{1}^{j_{1}}, \dots, \boldsymbol{\vartheta}_{M}^{j_{M}})$ and $\boldsymbol{a} = (a_{1}, \dots, a_{M})$. Since f_{LS} is a solution of the PDE by construction, the problem of finding a solution to the IBVP is reduced to match given initial and/or boundary conditions $\mathcal{B}_{1}, \dots, \mathcal{B}_{r}$, i.e. finding the optimal set of parameters \boldsymbol{a} and $\boldsymbol{\theta}$. To formalize this, we introduce the loss function:

$$\mathcal{L}(\boldsymbol{a}, \theta) := \sum_{k=1}^{r} \frac{1}{|\mathcal{X}_k|} \sum_{x \in \mathcal{X}_k} \left\| \mathcal{B}_k \left(x, f_{LS}(x; \boldsymbol{a}, \theta), \frac{\mathrm{d} f_{LS}(x; \boldsymbol{a}, \theta)}{\mathrm{d} \mathbf{n}} \right) \right\|_2^2$$
(29)

³We borrow this term from the Finite Element Method. However, this set will not necessarily be minimal, but we will span a solution-(sub)space by these "base solutions".

where $\mathcal{X}_k \subset \Gamma_k$ are finite sets of randomly sampled collocation points from the boundary parts $\Gamma_k \subset \partial \Omega$ according to section 2.2. The union $\mathcal{X} = \bigcup_{k=1}^r \mathcal{X}_k$ forms the training dataset and consists of L points $\mathcal{X} \subseteq \mathbb{R}^{L \times n}$ (rows are individual points $x \in \mathbb{R}^n$). Consequently, boundary conditions $\mathcal{B}_1, \ldots, \mathcal{B}_r$ define set of target values $\mathcal{Y} \in \mathbb{R}^{L \times m}$ at datapoints \mathcal{X} .

The seed solutions, the chosen transformations applied to them, and the number of base solutions are design choices of the model. The amplitudes a and transformation parameters θ serve as the optimizable parameters.

3.2 The LieSolver optimization algorithm

LIESOLVER determines an optimal linear combination $f_{LS}(x; \boldsymbol{a}, \theta) = \sum_i a_i f_i^{j_i}(x; \boldsymbol{\vartheta}_i^{j_i})$ via two stages. First, LIESOLVER employs greedy addition of the base solutions $f_i^{j_i}(x; \boldsymbol{\vartheta}_i^{j_i})$; it appends the active set \mathcal{A} with the base solution with the largest absolute cosine similarity to the current residual

$$r = \mathcal{Y} - f_{LS}(\mathcal{X}; \boldsymbol{a}, \boldsymbol{\theta}) \quad , \tag{30}$$

and updates amplitudes a with ridge least squares (LS). Here, $f_{LS}(\mathcal{X}; a, \theta)$ is to be understood as the natural extension of (28) to \mathcal{X} . Second, it employs variable projection to eliminate the linear amplitudes a and periodically refine only the nonlinear parameters θ with nonlinear least squares (NLLS).

Variable projection

By employing variable projection [12, 26], we eliminate the amplitudes a by solving the LS subproblem exactly for fixed θ ,

$$\boldsymbol{a}^{\star}(\theta) = \arg\min_{\boldsymbol{a}} \left(\| \boldsymbol{\mathcal{Y}} - F(\theta) \boldsymbol{a} \|_{2}^{2} + \lambda \| \boldsymbol{a} \|_{2}^{2} \right) = (F^{\top} F + \lambda I)^{-1} F^{\top} \boldsymbol{\mathcal{Y}} , \qquad (31)$$

where $f_{LS}(\mathcal{X}; \boldsymbol{a}, \theta)$ is represented as the matrix-vector product with the matrix $F(\theta) = [f_i^{j_i}(\mathcal{X}; \boldsymbol{\vartheta}_i^{j_i})]_{i=1}^M$ and $\lambda > 0$ is the ridge parameter. Substituting $\boldsymbol{a}^{\star}(\theta)$ back into minimization objective yields the reduced problem:

$$\theta^{\star} = \arg\min_{\theta} \|\mathcal{Y} - F(\theta) \, \boldsymbol{a}^{\star}(\theta)\|_{2}^{2} \quad , \tag{32}$$

which we minimize over allowed values of θ with NLLS⁴, specifically with bound-constrained trustregion reflective least squares. This reduces the optimization dimension to the nonlinear parameters, improves conditioning by solving the linear part exactly at each step, and stabilizes training.

Educated guess of base functions

The initial catalogue of bases S determines the expressivity of the constructed solution, and thus is crucial for performance. The bases should reproduce a wide range of patterns expected under the given PDE and initial-boundary data. Further, the parameter bounds and the chosen sampling rule (uniform or log-uniform) should cover relevant scales.

For example, for the heat equation, the effective choice includes scaled/shifted Fourier modes from a seed solution like $\sin(x)e^{-t}$, Gaussian blobs generated from a constant seed solution by applying diffusion/shift, and a hybrid that combines both behaviours.

⁴https://docs.scipy.org/doc/scipy/reference/generated/scipy.optimize.least_squares.html

The LieSolver algorithm

In conclusion to the details discussed above, we present the specific algorithm for LieSolver, which depends on the following inputs:

- Training data $\mathcal{X} \subset \partial\Omega \in \mathbb{R}^{L \times n}$ (rows are points $x \in \mathbb{R}^n$) and targets $\mathcal{Y} \in \mathbb{R}^{L \times m}$ on the IBC set
- A set of base solutions $S = \{f^1(x; \boldsymbol{\vartheta}^1), \dots, f^N(x; \boldsymbol{\vartheta}^N)\}$. Each f^i is defined by a seed solution and an ordered list of transforms with parameter bounds and a sampling rule (27). Composing them yields a symbolic expression and a fast numeric evaluator $f_{LS}(x; \boldsymbol{a}, \boldsymbol{\theta})$.
- Hyperparameters:

```
- mse_tol: early stopping threshold on training MSE
- max_terms: maximum number of bases in the active set \mathcal{A}
- P: parameter samples per base per addition for candidate scoring
- R: number of additions between NLLS refinements
- \lambda: ridge parameter for \ell_2 regularization in least squares
- sampling seed
```

Algorithm 1 LieSolver

```
Input: data (\mathcal{X}, \mathcal{Y}); base solutions \mathcal{S}; hyperparameters mse_tol, max_terms, P, R, \lambda
Output: learned bases \mathcal{A} = \{(f_i^{j_i}, \hat{\boldsymbol{\vartheta}}_i^{j_i})\}_{i=1}^M, amplitudes \boldsymbol{a}; predictor \hat{f}(x) = \sum_{i=1}^M a_i f_i^{j_i}(x; \hat{\boldsymbol{\vartheta}}_i^{j_i})
  1: \mathcal{A} \leftarrow \emptyset, \boldsymbol{a} \leftarrow [\ ], r \leftarrow \mathcal{Y}, \text{mse} \leftarrow ||r||_2^2/L
  2: while mse > mse_tol and |A| < max_terms do
                  for q = 1 to R do
                                                                                                                                                                                       \triangleright Add R base terms to \mathcal{A}
  3:
                          for each i \in \{1, \dots, N\} do sample \{\vartheta_p^i\}_{p=1}^P within bounds
                                                                                                                                                                          ▶ Sample and score candidates
  4:
  5:
                                   for p = 1 to P do
   6:
                                          \begin{aligned} & v_{i,p} \leftarrow f^i(\mathcal{X}; \boldsymbol{\vartheta}_p^i) \\ & s_{i,p} \leftarrow \frac{|\langle r, v_{i,p} \rangle|}{\|r\|_2 \, \|v_{i,p}\|_2} \end{aligned}
   7:
  8:
                                   end for
  9:
10:
                          end for
                          (i^{\star}, \boldsymbol{\vartheta}^{\star}) \leftarrow \arg \max_{i,p} s_{i,p}
append f_{i^{\star}}(\cdot; \boldsymbol{\vartheta}^{\star}) to \mathcal{A}
11:
12:
                                                                                                                                                                              \triangleright Best candidate added to \mathcal{A}
                          F \leftarrow [f_i^{j_i}(\mathcal{X}; \hat{\boldsymbol{\vartheta}}_i^{j_i})]_{i \in \mathcal{S}} \\ \boldsymbol{a}^* \leftarrow \arg\min_{\boldsymbol{a}} \ \|\mathcal{Y} - F\boldsymbol{a}\|_2^2 + \lambda \|\boldsymbol{a}\|_2^2
13:
                                                                                                                                                                                               \triangleright Amplitudes a by LS
14:
                          \boldsymbol{a} \leftarrow \boldsymbol{a}^{\star}; \quad r \leftarrow \mathcal{Y} - F\boldsymbol{a}; \quad \text{mse} \leftarrow ||r||_2^2/L
15:
                          if mse \le mse\_tol \ or \ |A| = max\_terms \ then
16:
                                   return
17:
                          end if
18:
                  end for
19:
                 \begin{aligned} & \theta^{\star} \leftarrow \arg\min_{\theta} \ \frac{1}{2} \| \mathcal{Y} - F(\theta) \, \boldsymbol{a}^{\star}(\theta) \|_{2}^{2} \\ & \boldsymbol{a} \leftarrow \boldsymbol{a}^{\star}(\theta^{\star}); \quad r \leftarrow \mathcal{Y} - F(\theta^{\star}) \boldsymbol{a}; \quad \text{mse} \leftarrow \|r\|_{2}^{2}/L \end{aligned}
                                                                                                                                                                                         \triangleright Refine \theta by NLLS (32)
20:
21:
                                                                                                                                                                                   \triangleright Amplitudes a by LS (31)
22: end while
```

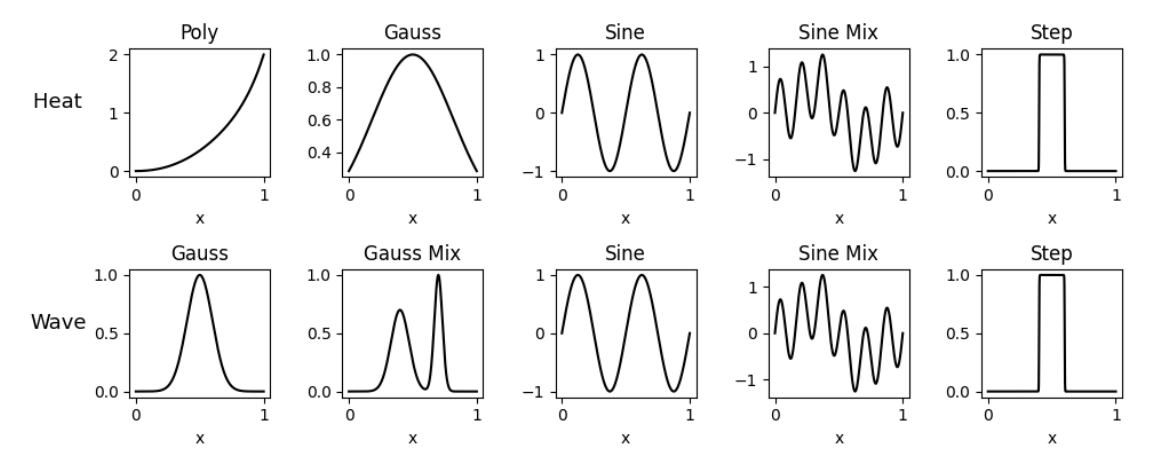


Figure 1: Initial conditions (solution shapes at t = 0) for the test cases for the heat (top row) and the wave (bottom row) equations.

Code availability

The Python implementation is available at https://github.com/oduwancheekee/liesolver.

4 Experiments and results

To evaluate performance and demonstrate the capabilities of the model, we apply LIESOLVER to several IBVPs for the one-dimensional heat equation, and the one-dimensional wave equation and compare its performance with standard PINNs and demonstrate its efficiency. LIESOLVER outperforms PINNs in our benchmarks regarding accuracy as well efficiency. Since both of these problems are well-posed, we can demonstrate the relation between accuracy and test loss as stated in section 2.2.

4.1 Experimental setup

In our experiments, we report the mean squared error (MSE) on the IBC data and the relative L_2 error (L2RE) on the space-time grid in the domain Ω . Since all targets are on the order of unity in their magnitude, MSEs are comparable across all problem instances. Unless stated otherwise, we use $P=1000,\ R=5,\ \text{nfev_global}=4$ (number of trust-region reflective steps in global refine), $\lambda=10^{-1},\ L=3000,\ \text{mse_tol}=10^{-6},$ for a robust, empirically determined configuration in LIESOLVER.

For the heat equation $\mathcal{D}(x,t,u^{(2)})=u_t-u_{xx}$, we use $(x,t)\in(0,1)\times(0,0.1)$ as the domain, and we consider five different profiles polynomial, Gaussian, sine, sine mix, and step for the initial condition $u(x,0)=u_0(x)$, which are shown in figure 1. The boundary conditions are set to constant values defined by the initial condition $u(0,t)=u_0(0)$ and $u(1,t)=u_0(1)$. Similarly, for the wave equation $\mathcal{D}(x,t,u^{(2)})=u_{tt}-u_{xx}$, we set $(x,t)\in(0,1)\times(0,1)$ with u(0,t)=u(1,t)=0, $u_t(x,0)=0$ and consider the five IC profiles sine, sine mix, Gaussian, Gaussian mix, and step, also depicted in figure 1.

Reference solution

In order to compare the predictions of LieSolver, we compute a reference ground truth solutions by expanding the initial data in a sine basis according to [4]. For the heat equation with Dirichlet BC, we set $b_L = u(0,0)$ and $b_R = u(1,0)$ and define $w(x) = b_L + (b_R - b_L) x$ so that $v_0(x) = u(x,0) - w(x)$ satisfies homogeneous Dirichlet conditions. We sample v_0 at the interior points $x_m = \frac{m}{M+1}$ for $m = 1, \ldots, M$ and obtain the coefficients A_m via orthonormal projection onto $\sin(m\pi x)$. The solution is

$$f_{\text{ref}}(x,t) = w(x) + \sum_{m=1}^{M} A_m \sin(m\pi x) e^{-m^2 \pi^2 t}.$$
 (33)

For the wave equation with homogeneous Dirichlet boundaries, we sample u(x,0) and $u_t(x,0)$ at the same interior points x_m and compute A_m and B_m by orthonormal projection onto $\sin(m\pi x)$. The solution is then given by

$$f_{\text{ref}}(x,t) = \sum_{m=1}^{M} \left[A_m \cos(m\pi t) + \frac{B_m}{\omega_m} \sin(m\pi t) \right] \sin(m\pi x). \tag{34}$$

Base solutions

LIESOLVER requires an educated choice of parametrized base solutions $f(x; \vartheta)$ (see section 3.2). For the one-dimensional heat equation, we can use the constant solution $f_{\text{seed},1}(x,t) \equiv 1$ and $f_{\text{seed},2}(x,t) = e^{-t} \sin x$ as possible seed solutions. Based on these seed solutions, we employ three complementary base solutions generated by Lie symmetries (18) – (23) of the heat equation:

- $f^1(x,t;\vartheta^1) = T^4_{\vartheta_2} \circ T^1_{\vartheta_1} \circ (e^{-t}\sin x)$: scaled/shifted Fourier mode (variable phase/frequency).
- $f^2(x,t;\vartheta^2) = T^1_{\vartheta_2} \circ T^6_{\vartheta_1} \circ (1)$: diffusion-generated Gaussian blob (variable center and width).
- $f^3(x,t;\vartheta^3) = T^1_{\vartheta_4} \circ T^6_{\vartheta_3} \circ T^4_{\vartheta_2} \circ T^1_{\vartheta_1} \circ (e^{-t}\sin x)$: Gaussian blob modulated by a scaled/shifted sine.

Figure 2 illustrates the variety of base solutions chosen to solve the heat equation.

For the one-dimensional wave equation, we identify a subgroup of the Lie symmetry group and consider two transformations: spatial translation T^1 and spatiotemporal scaling T^2 :

$$T^1_{\vartheta}: f(x,t) \mapsto f(x-\vartheta,t)$$
 (35)

$$T_{\vartheta}^{2}: f(x,t) \mapsto f(e^{\vartheta}x, e^{\vartheta}t) . \tag{36}$$

We employ them to compose the following two base solutions for the wave equation:

- $f^1(x, t; \vartheta^1) = T_{\vartheta_2}^2 \circ T_{\vartheta_1}^1 \circ (\sin x \cos t)$: scaled/shifted standing-wave (variable phase/frequency), which is suitable for homogeneous Dirichlet BCs.
- $f^2(x,t;\vartheta^2) = T^1_{\vartheta_2} \circ T^2_{\vartheta_1} \circ (e^{-(x-t)^2} + e^{-(x+t)^2})$: Gaussian pattern (variable centre and width). Zero velocity IC enables us to use travelling blob pair instead of just one travelling blob.

4.2 PINN Baseline Setup

We use a standard fully connected neural network $f_{PINN}: \mathbb{R}^2 \to \mathbb{R}$ with input (x, t), tanh activation function and where the number of layers and their width is specified in table 2 in alignment with

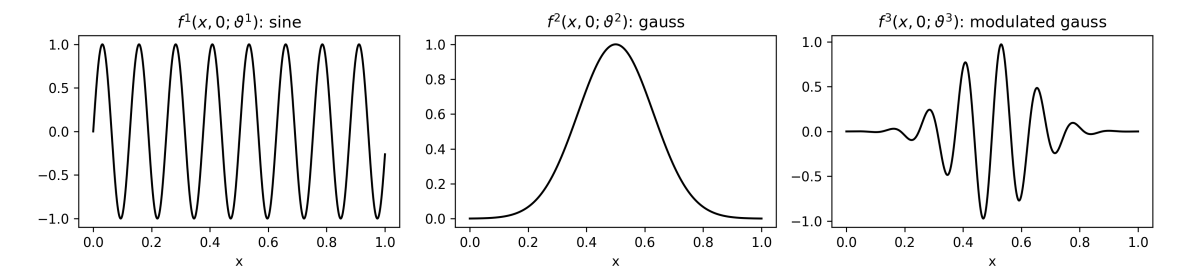


Figure 2: Representative base families for one-dimensional heat equation at t = 0: f^1 (sine), f^2 (Gaussian), and f^3 (Gaussian modulated by a sine) with illustrative parameter choices.

[40]. The loss combines the PDE residual, a several weighted IBC terms:

$$\mathcal{L}_{res}(\boldsymbol{w}) = \frac{1}{N_r} \sum_{(x_k, t_k) \in X_r} \left(f_{PINN, t}(x_k, t_k, \boldsymbol{w}) - f_{PINN, xx}(x_k, t_k, \boldsymbol{w}) \right)^2, \tag{37}$$

$$\mathcal{L}_{\text{ICBC}}(\boldsymbol{w}) = \frac{1}{L} \sum_{(x_j, t_j) \in \mathcal{X}, y_j \in \mathcal{Y}} (f_{\text{PINN}}(x_j, t_j, \boldsymbol{w}) - y_j)^2,$$
(38)

$$\mathcal{L}_{\text{vel}}(\boldsymbol{w}) = \frac{1}{N_{\text{vel}}} \sum_{(x_j, t_j) \in \mathcal{X}_{\text{vel}}} (f_{\text{PINN}, t}(x_j, t_j, \boldsymbol{w}))^2,$$
(39)

$$\mathcal{L}(\boldsymbol{w}) = \mathcal{L}_{res}(\boldsymbol{w}) + w_{ICBC}\mathcal{L}_{ICBC}(\boldsymbol{w}) + \mathcal{L}_{vel}(\boldsymbol{w}) . \tag{40}$$

Here, $\mathcal{X}_r \subset \Omega$ are the collocation points in the domain, while \mathcal{X} and \mathcal{Y} are the same sets of IBC points and targets used for LieSolver. The loss weight w_{ICBC} is tuned to mitigate ill-conditioning and facilitate training (see table 2). We warm up with Adam for 1000 iterations and then train with L-BFGS until convergence or optimizer stall.

4.3 Results

Table 1 summarizes representative runs of LIESOLVER for the considered IBVPs, while table 2 reports the corresponding PINN runs. For all ICs except the step IC, LIESOLVER reliably attains IBC MSE values of order 10^{-6} using between 5 and 40 bases. The step IC requires more bases due to its sharp jump. PINNs match LIESOLVER in terms of attained MSE only on the easiest cases, but falls short on the more challenging ICs. The sine mix IC requires a larger 6×100 PINN. Notably, the step IC does not reach the target tolerance even with larger PINN models.

LIESOLVER is about one to two orders of magnitude faster than PINN across the considered cases. However, its runtime⁵ increases sharply as the number of bases grows. Configurations with fewer than 20 bases train within 10 s, 40 bases – within 40 to 60 s, and around 80 bases take 200 to 300 s. This growth is determined by the global parameter refinement stage. More targeted refinement strategies could mitigate this bottleneck.

The choice of base solutions strongly influences performance. Employing sine and Gaussian bases, LieSolver naturally fits IC profiles with similar sine and Gaussian patterns and reaches

⁵All experiments were run on an Intel Core Ultra 7 165H CPU with 11 cores and 16 GiB RAM.

Table 1: Representative LieSolver results for the one-dimensional heat and wave equations, reporting accuracy, runtime and model complexity.

PDE	IBC Type	MSE (IBC)	L2RE (domain)	Runtime [s]	$N_{ m base_terms}$	$N_{ m parameters}$
Heat	polynomial	$5.6 \cdot 10^{-7}$	$4.8 \cdot 10^{-4}$	43	40	112
	Gaussian	$7.8 \cdot 10^{-7}$	$8.6 \cdot 10^{-4}$	5	11	32
	sine	$1.8 \cdot 10^{-7}$	$1.6 \cdot 10^{-3}$	3	5	14
	sine mix	$2.3 \cdot 10^{-7}$	$1.9 \cdot 10^{-3}$	5	10	28
	step	$8.9 \cdot 10^{-6}$	$4.6 \cdot 10^{-3}$	91	58	196
Wave	Gaussian	$7.7 \cdot 10^{-7}$	$3.8 \cdot 10^{-3}$	6	13	26
	Gaussian mix	$6.1 \cdot 10^{-7}$	$4.0 \cdot 10^{-3}$	44	40	80
	sine		$2.1 \cdot 10^{-4}$	3	5	10
	sine mix	$7.6 \cdot 10^{-7}$	$2.0 \cdot 10^{-3}$	5	9	18
	step	$8.3 \cdot 10^{-7}$	$5.1 \cdot 10^{-3}$	197	80	160

Table 2: Representative PINN results for the one-dimensional heat and wave equations, reporting accuracy, runtime, and model configuration.

PDE	IBC Type	MSE (IBC)	L2RE (domain)	Runtime [s]	Training iterations	Network	IBC weight
Heat	polynomial	$9.0 \cdot 10^{-7}$	$4.8 \cdot 10^{-4}$	110	3500	4×50	10^{3}
	Gaussian	$3.2 \cdot 10^{-7}$	$4.9 \cdot 10^{-4}$	100	3500	4×50	10^{3}
	sine	$7.8 \cdot 10^{-7}$	$5.0 \cdot 10^{-3}$	160	4200	4×50	10^{3}
	sine mix	$4.6 \cdot 10^{-6}$	$1.9 \cdot 10^{-2}$	1580	9700	6×100	10^{5}
	step	$1.8 \cdot 10^{-3}$	$2.2 \cdot 10^{-1}$	320	3000	6×100	10^{5}
Wave	Gaussian	$1.5 \cdot 10^{-7}$	$1.6 \cdot 10^{-3}$	1100	7300	4×50	10^{3}
	Gaussian mix	$2.7 \cdot 10^{-6}$	$8.2 \cdot 10^{-3}$	2500	17000	4×50	10^{3}
	sine	$2.0 \cdot 10^{-7}$	$8.5 \cdot 10^{-4}$	1200	7800	4×50	10^{3}
	sine mix	$8.2 \cdot 10^{-5}$	$1.8 \cdot 10^{-2}$	11000	21000	6×100	10^{3}
	step	$7.2 \cdot 10^{-5}$	$4.5 \cdot 10^{-2}$	900	6800	4×50	10^{3}

the target MSE in under a minute. The step IC remains a challenging stress test and highlights model capability. In the following, we discuss three representative cases that illustrate LieSolver behaviour.

Heat equation with Gaussian IC

Figure 3 shows the evolution of the IBC MSE as a function of the number of added bases. The greedy stage begins with a Gaussian base f^2 that already captures most of the IC (MSE $\sim 10^{-3}$), followed by several Fourier-like additions (f^1 and f^3) that enforce the Dirichlet BCs. The first global refinement stage (after 5 bases) yields a one-order-of-magnitude drop in MSE; the target tolerance ($< 10^{-6}$) is met after 11 bases. Details on performance metrics and computation are provided in table 1. Moreover, we confirm the considerations from section 2.2 that there is an upper bound for the ratio between MSE on the domain and the test MSE on the IBCs as indicated in (13). Hence, we show that the loss serves as a reliable metric for the overall domain accuracy.

Figure 4 and figure 5 compare the model prediction with the ground truth in the domain and on the IBCs, respectively. The IBC plots include a decomposition into the weighted base terms, revealing dominant Gaussian-like contributors for the IC profile and additional base terms that fit the BCs. For reference, a vanilla PINN also fits this smooth case to an IBC MSE $< 10^{-6}$ (figure 6), albeit requiring a longer runtime, as indicated in table 2.

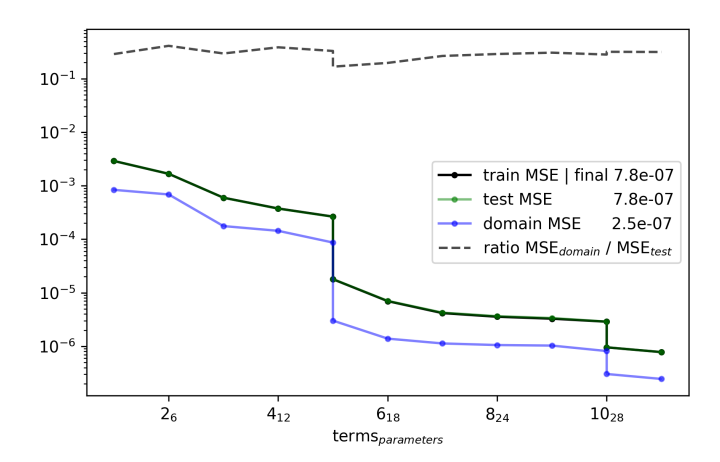


Figure 3: Fit progress of LieSolver for the heat equation with Gaussian IC: IBC MSE is shown as a function of the number of added bases. The vertical drops correspond to the global refinement steps.

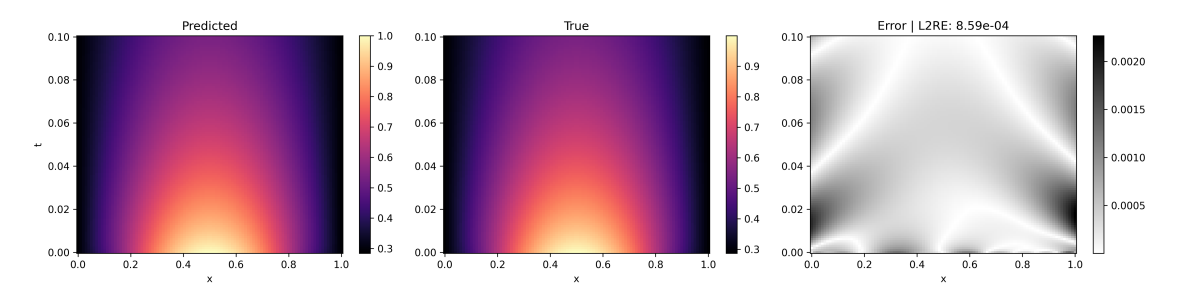


Figure 4: 2D domain fields (prediction, ground truth, and error) for the heat equation with Gaussian IC.

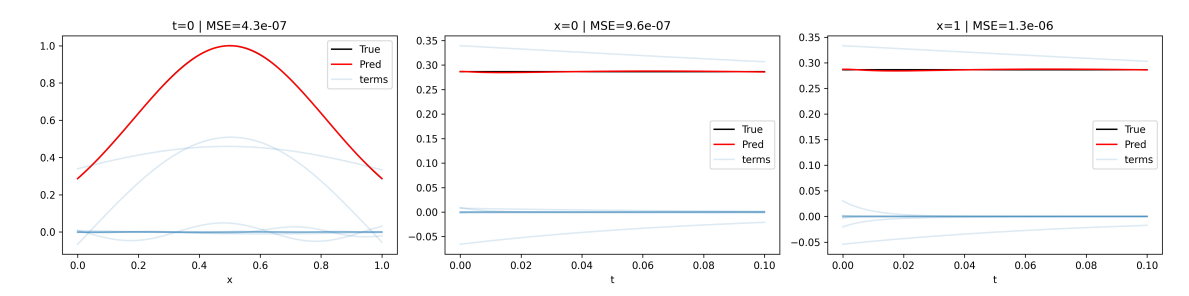


Figure 5: IBC fits for the heat equation with Gaussian IC, including the decomposition into weighted base contributions. The transparent blue curves depict the individual contributions.

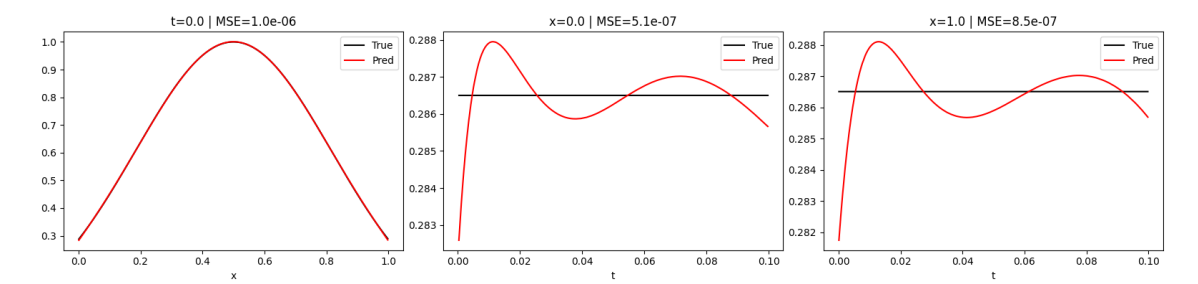


Figure 6: Comparison of the PINN prediction with the ground truth on the IBCs for the heat equation with Gaussian IC.

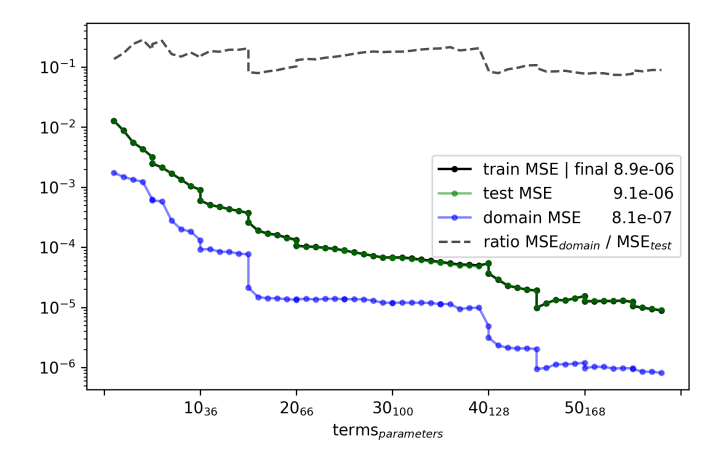


Figure 7: Training progress of LIESOLVER for the heat equation with step IC. IBC MSE is shown as a function of the number of added bases.

Heat equation with step IC

The step IC represents the most challenging case due to the jump in the profile. Figure 7 highlights three regimes of LieSolver optimization: (i) rapid improvement to MSE $\approx 10^{-4}$ within 15 bases, (ii) a stall where additional bases bring limited improvement, and (iii) resumed progress after 40 bases culminating in $< 10^{-5}$ with 58 bases. Figures 8 and 9 show that the dominant residual is localized near the initial jump. Despite IBC MSE being higher than the target, the domain L2RE reaches $4.6 \cdot 10^{-3}$, which is comparable to other IC cases. The decomposition in figure 9 is less interpretable than in the Gaussian case due to the large number modulated base contributions. A standard PINN plateaus around 10^{-3} IBC MSE (figure 10) and $\sim 10^{-1}$ L2RE in the domain. The transition from an extremely sharp IC to a rapidly smoothening solution in the domain is hard for PINNs. Even larger networks fail to capture this dependency and underperform relative to the LIESOLVER.

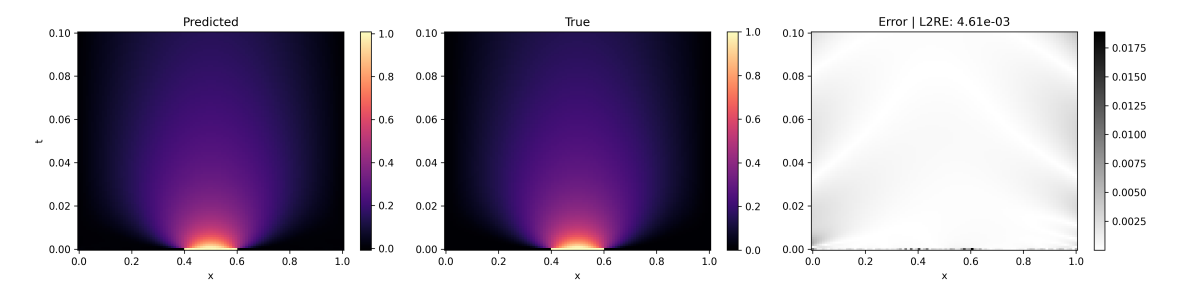


Figure 8: 2D domain fields (prediction, ground truth, and error) for the heat equation with step IC.

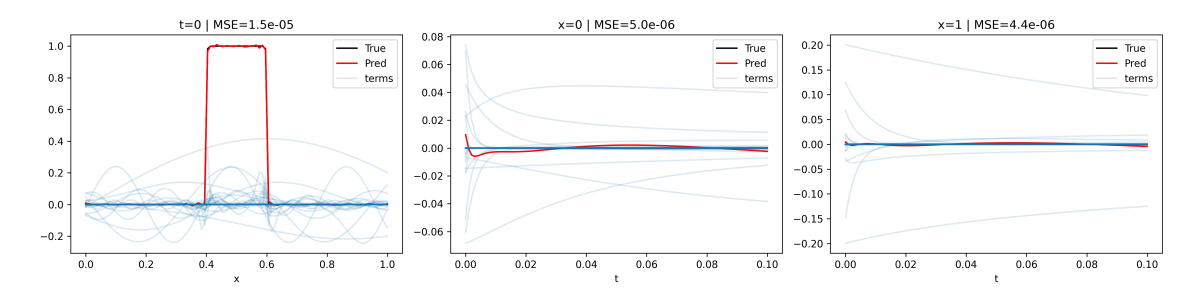


Figure 9: IBC fits for the heat equation with step IC, including the decomposition into weighted base contributions. The transparent blue curves depict the individual contributions.

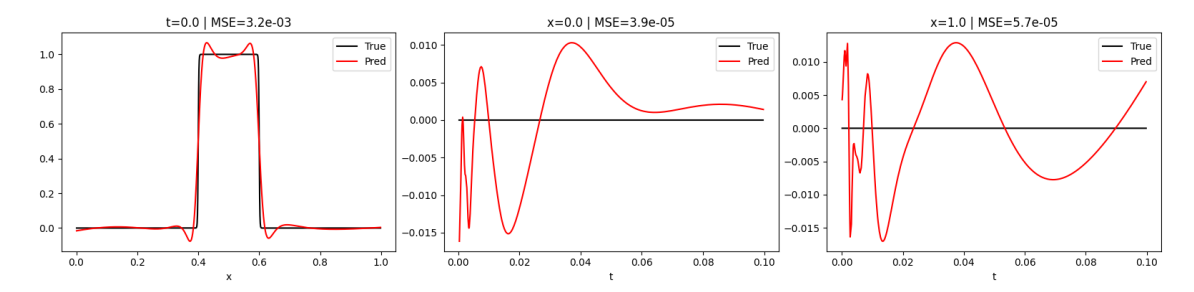


Figure 10: Comparison of the PINN prediction with the ground truth on the IBCs for the heat equation with step IC.

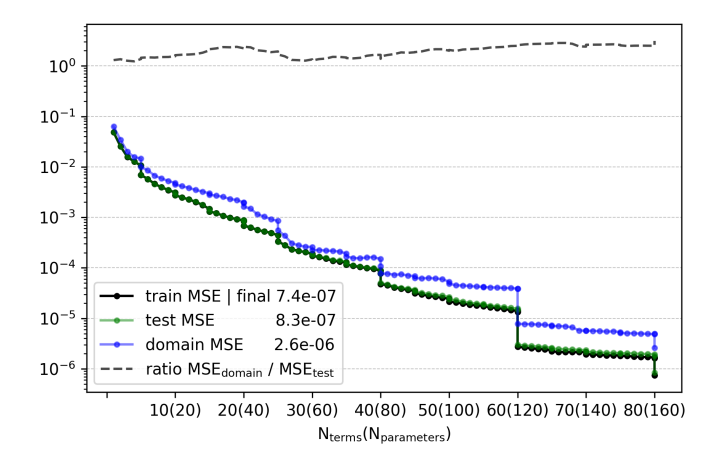


Figure 11: Training progress of LIESOLVER for the wave equation with step IC. IBC MSE is shown as a function of the number of added bases.

Wave equation with step IC

Figure 11 illustrates effective handling of the challenging wave PDE with a sharp step IC by LieSolver. A Global parameter refinement at 60 and 80 base terms yields pronounced drops in MSE. With a sufficient number of active bases, the optimizer can adjust them effectively and achieve lower error. Figure 13 shows that the solution is primarily composed of Fourier sine modes with localized Gaussian corrections. During optimization, the greedy stage first selects sine bases to fit the dominant high-amplitude oscillatory component. As the remaining residual becomes localized and irregular, the algorithm increasingly adds Gaussian bases to correct for edges and boundary regions.

With Gaussian bases, the residual is fitted in two steps. First, the model picks a positive pulse propagating into the domain. Second, it adds opposite-sign contributions to compensate for positive pulses at the boundaries and to reproduce the reflected wave (see the BC plots, middle and right subplots in figure 13). This structure is straightforward for the optimizer, and further MSE reduction is attainable with additional bases and parameters refinement. The domain plot is presented in figure 12. The model achieves an L2RE of $5.1 \cdot 10^{-3}$ on the domain. The PINN handles the step IC better for the wave equation (Figure 14) than for the heat equation (Figure 10). The reason is that the wave PDE lacks parabolic smoothing; there is no abrupt transition from a sharp IC to a rapidly smoothed interior solution. Nevertheless, it does not resolve the sharp features sufficiently well and underperforms relative to LIESOLVER, achieving only an L2RE of $4.5 \cdot 10^{-2}$ in the domain.

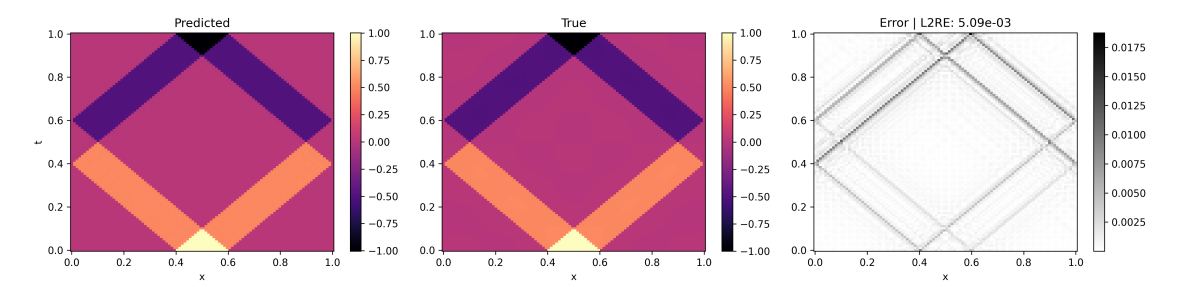


Figure 12: 2D domain fields (prediction, ground truth, and error) for the wave equation with step IC.

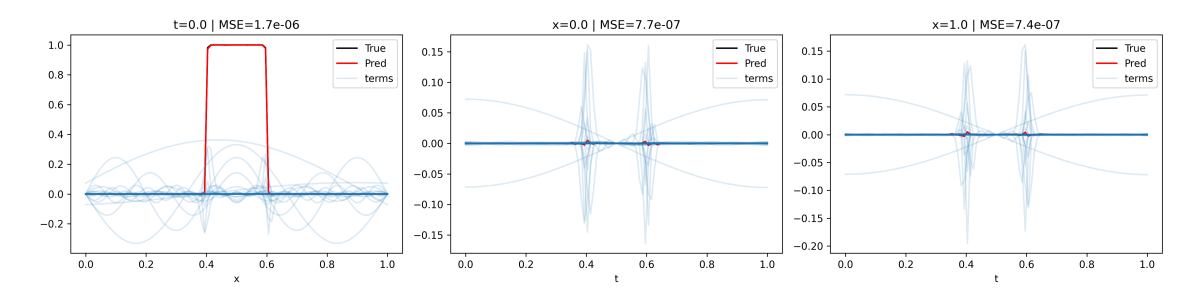


Figure 13: IBC fits for the wave equation with step IC, including the decomposition into weighted base contributions. The transparent blue curves depict the individual contributions.

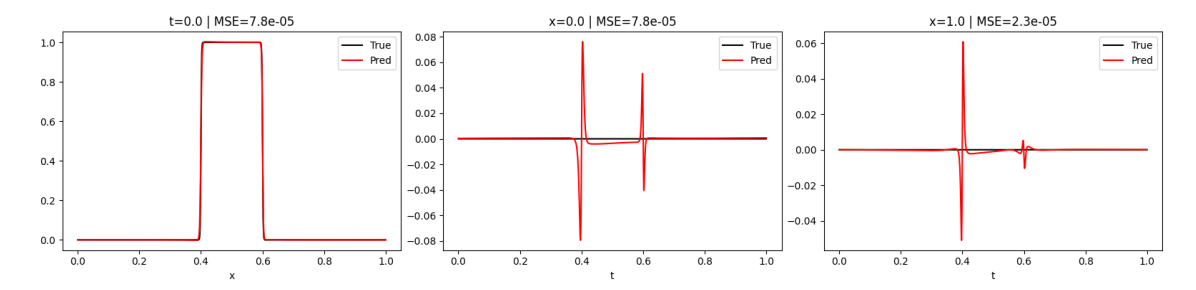


Figure 14: Comparison of the PINN prediction with the ground truth on the IBCs for the wave equation with step IC.

5 Conclusion

Using Lie symmetries, we generate parametrized functions that exactly solve the corresponding PDE. By incorporating the underlying symmetry structures directly into the model, solving initial-boundary value problems reduces to optimizing these parameters to satisfy the initial-boundary conditions (IBCs). Thus, for any parameter values, the model will solve the PDE by design. Focusing on the common case of linear homogeneous PDEs, we introduced LIESOLVER, which represents the solution as a linear combination of Lie-symmetry-generated base solutions whose linear amplitudes and symmetry parameters are learned from the IBCs. LIESOLVER constructs this representation incrementally by greedily adding the base function that yields the largest MSE reduction at each step. We use variable projection to eliminate the linear amplitudes via least squares (LS), yielding a reduced problem in the symmetry parameters, which we solve with a bound-constrained nonlinear least squares (NLLS).

The most notable difference between PINNs [32] and our proposed method is that we incorporate PDEs into the model's structure rather than including the PDE as a loss term in the optimization procedure. This approach offers several advantages: in our model, the loss function effectively serves as a faithful indicator of predictive accuracy, providing a reliable measure of the progress of training. Specifically, a decrease in the test loss – unlike in PINNs – always indicates an improvement in accuracy. In addition, this property implies the existence of rigorous error bounds for well-posed IBVPs.

Moreover, these tailor-made models use comparatively few parameters, which yields significant computational speedups without sacrificing expressivity. This also enables robust optimization with nonlinear least squares (NLLS), improving predictive accuracy. Across our benchmarks on 1D heat and wave equations with Dirichlet boundary conditions, LIESOLVER achieved IBC MSE below 10^{-6} with fewer than 40 bases (about 100 parameters) for smooth ICs and ran one to two orders of magnitude faster than PINNs. For the step IC with a sharp jump it required more bases yet still attained domain L2RE on the order of 10^{-3} , whereas PINNs plateaued between 10^{-2} and 10^{-1} (tables 1 and 2). Furthermore, the compact models provably satisfy the underlying physics (that is, the PDE), which enables the prediction to be expressed as a sparse, analytical expression, thereby enhancing interpretability.

Despite the notable advantages of using Lie symmetries, it is important to acknowledge the limitations of our approach. Currently, LieSolver applies only to linear homogeneous PDEs. Although this encompasses a large class of important problems, we aim to generalize our framework in future work. Another drawback is that, for every PDE, the Lie symmetries and at least one seed solution must be derived. However, Lie symmetries can be determined algorithmically and for the most standard problems, they can also be found in the literature. Finding seed solutions is trivial for the class of linear homogeneous PDEs and remains feasible in more general cases. A further weakness is that the performance of LieSolver heavily depends on the chosen set of base solutions, an aspect that requires further investigation to improve automatization. However, as is the case in conventional neural networks, performance highly depends on various design choices. Nonetheless, in our approach, the loss constitutes a rigorous means to assess whether a particular choice of base solution is effective or needs to be extended, providing useful criteria for these design choices. It is also important to note that we have tested LieSolver only on a limited number of problems. Therefore, more extensive studies will be necessary in future work.

From the aforementioned, several next steps emerge naturally: a more detailed analysis of Lie-

SOLVER on various problems, an automated selection of base solutions, as well as an extension to more general classes of PDEs. For the latter task, genetic algorithms appear to be a promising direction. By pursuing these steps, we aim to enhance the capabilities and applicability of LIESOLVER and provide an interpretable, reliable and efficient solver of IBVPs for general PDEs.

Code availability

The Python implementation is available at https://github.com/oduwancheekee/liesolver.

Acknowledgements: The authors would like to thank Aleksander Krasowski, Théo Tyburn, Gleb Wassiltschuk and Moritz Weckbecker for helpful discussions.

A Appendix

A.1 Computation of Lie symmetry groups

In addition, to the short summary in section 2, we will provide a brief overview of how to compute the symmetry group of a system. To keep the description as short as possible, we will omit many details and focus on a practical guide for calculating the symmetry group. For further details, we recommend [31, ch. 2], which the following is oriented towards. Before stating the so-called infinitesimal criterion, which is the key concept for the determination of symmetry groups, we have to introduce some further definitions.

Every Lie group G is related to a so-called $Lie\ algebra\ \mathfrak{g}$, which is defined to be the tangent space of G at its identity element (see e.g. [10] for further details). Due to their vector space structure, it is often much more convenient to work with the Lie algebra \mathfrak{g} , instead of the Lie group G. By Lie's third theorem [31, thm. 1.54] there is a one to one correspondence between finite-dimensional Lie algebras \mathfrak{g} and connected Lie groups G. Thus, we will lose no generality, when considering Lie algebras. Elements of the Lie algebras are also called *infinitesimal generators* of a Lie group.

A system of PDEs $\mathcal{D}(x, u^{(d)})$ is called to be of maximal rank, if its Jacobian $J_{\mathcal{D}}(x, u^{(d)})$ with respect to all variables has the maximal rank p, whenever $\mathcal{D}(x, u^{(d)}) = 0$. E.g., $\mathcal{D}(x, u^{(2)}) = u_t - u_{xx}$ has Jacobian $J_{\mathcal{D}}(x, t; u, u_x, u_t, u_{xx}, u_{xt}, u_{tt}) = (0, 0; 0, 0, 1, -1, 0, 0)$, which is of maximal rank, whereas $\mathcal{D}(x, u^{(2)}) = (u_t - u_{xx})^2$ is not of maximal rank.

Theorem A.1 [Infinitesimal criterion, see [31, thm. 2.31]]: Let \mathcal{D} be a system of PDEs with maximal rank defined over $M \subseteq X \times U$ and let G be a local group of transformations acting on M. If

$$\operatorname{pr}^{(d)} \mathbf{v}[\mathcal{D}(x, u^{(d)})] = 0, \quad \text{whenever } \mathcal{D}(x, u^{(d)}) = 0$$
(41)

holds for any infinitesimal generator \mathbf{v} of G, then G is a symmetry group of \mathcal{D} .

In fact, this theorem gives us a computable criterion to determine the infinitesimal generators \mathbf{v} of the symmetry group. To evaluate (41), we also need to prolong a vector fields, which can be

computed for a general vector field

$$\mathbf{v} = \sum_{i=1}^{n} \xi^{i}(x, u) \frac{\partial}{\partial x_{i}} + \sum_{k=1}^{m} \phi_{k}(x, u) \frac{\partial}{\partial u^{k}}$$
(42)

by [31, thm. 2.36 and prop. 2.35]

$$\operatorname{pr}^{(d)} \mathbf{v} = \mathbf{v} + \sum_{k=1}^{m} \sum_{J \in [n]^{d} \setminus \emptyset} \phi_{k}^{J}(x, u^{(d)}) \frac{\partial}{\partial u_{J}^{k}}$$
(43)

with

$$\phi_k^J(x, u^{(d)}) = D_J \left(\phi_k - \sum_{i=1}^n \xi^i u_i^k \right) + \sum_{i=1}^n \xi^i u_{J \cup \{i\}}^k$$
(44)

and the total derivatives

$$D_{\{j_1,\dots,j_l\}} = D_{j_1} \cdots D_{j_l} \quad \text{with} \quad D_j = \frac{\partial}{\partial x_j} + \sum_{k=1}^m \sum_{I \in [n]^d} u_{J \cup \{j\}}^k \frac{\partial}{\partial u_J^k} \quad . \tag{45}$$

Let us illustrate theorem A.1 and these relatively lengthy formulas through a practical example.

Example A.2 [1d-heat equation]: Consider the heat equation

$$\mathcal{D}(x, u^{(2)}) = u_t - u_{xx} \tag{46}$$

with n=2, m=1, p=1 and d=2. Applying (43) and (41) to a generic vector field

$$\mathbf{v} = \xi(x, t, u) \frac{\partial}{\partial x} + \tau(x, t, u) \frac{\partial}{\partial t} + \phi(x, t, u) \frac{\partial}{\partial u}$$
(47)

we will obtain the infinitesimal criterion for symmetry groups as

$$\phi^t - \phi^{xx} = 0 \quad \text{whenever} \quad u_t = u_{xx} \quad . \tag{48}$$

To resolve the functions ϕ^t and ϕ^{xx} , we get by application of equations (44) and (45)

$$\phi^{t} = D_{t}(\phi - \xi u_{x} - \tau u_{t}) + \xi u_{xt} + \tau u_{tt} = D_{t}\phi - u_{x}D_{t}\xi - u_{t}D_{t}\tau$$

$$= \phi_{t} - \xi_{t}u_{x} + (\phi_{u} - \tau_{t})u_{t} - \xi_{u}u_{x}u_{t} - \tau_{u}u_{t}^{2}$$
(49)

and

$$\phi^{xx} = D_x^2 (\phi - \xi u_x - \tau u_t) + \xi u_{xxx} + \tau u_{xxt}
= D_x^2 \phi - u_x D_x^2 \xi - u_t D_x^2 \tau - 2u_{xx} D_x \xi - 2u_{xt} D_x \tau
= \phi_{xx} + (2\phi_{xu} - \xi_{xx}) u_x - \tau_{xx} u_t + (\phi_{uu} - 2\xi_{xu}) u_x^2 - 2\tau_{xu} u_x u_t - \xi_{uu} u_x^3
- \tau_{uu} u_x^2 u_t + (\phi_u - 2\xi_x) u_{xx} - 2\tau_x u_{xt} - 3\xi_u u_x u_{xx} - \tau_u u_t u_{xx} - 2\tau_u u_x u_{xt} .$$
(50)

Since $\phi^t = \phi^{xx}$ has to hold independently of the value of derivatives of u, we can compare them term-wise. When using in addition that $u_t = u_{xx}$, we get the following system of equations, which are often called the *determining equations*:

(i)
$$\phi_t = \phi_{xx}$$
 (vi) $-\xi_u = -2\tau_{xu} - 3\xi_u$

(ii)
$$-\xi_t = 2\phi_{xu} - \xi_{xx}$$
 (vii) $0 = -\tau_{uu}$

(iii)
$$0 = \phi_{uu} - 2\xi_{xu}$$
 (viii) $-\tau_u = -\tau_u$

$$(iv) 0 = -\xi_{uu} \qquad (ix) 0 = -2\tau_x$$

(v)
$$\phi_u - \tau_t = -\tau_{xx} + \phi_u - 2\xi_x$$
 (x) $0 = -2\tau_u$

In order to find the most general infinitesimal generator \mathbf{v} from (42), we have to solve this system, to determine the functions $\xi(x,t,u), \tau(x,t,u)$ and $\phi(x,t,u)$. From (ix) and (x), we get that $\tau = \tau(t)$ depends only on t. In combination with (vi), ξ will not depend on u. Hence, (v) takes the form $\tau_t = 2\xi_x$, which implies $\xi(x,t) = \frac{1}{2}\tau_t x + \gamma(t)$ for some function γ . Therefore, using (iii), ϕ will only linearly depend on u, i.e., $\phi(x,t,u) = \alpha(x,t) + \beta(x,t)u$ for some functions α, β . Hence, we have used every equation except (i) and (ii), which takes the form

(i)
$$\alpha_t = \alpha_{xx}, \ \beta_t = \beta_{xx}$$
 (ii) $-\frac{1}{2}\tau_{tt}x - \gamma_t = 2\beta_x$

By integrating (ii) w.r.t. x, we get $\beta(x,t) = -\frac{1}{8}\tau_{tt}x^2 - \frac{1}{2}\gamma_t x + \rho(t)$. Comparing with (i), we get $\tau_{ttt} = 0$, $\gamma_{tt} = 0$ and $\rho_t = -\frac{1}{4}\tau_{tt}$. Hence, $\tau(t) = 4c_6t^2 + 2c_4 + c_2$ is a quadratic function, $\gamma(t) = 2c_5t + c_1$ and $\rho(t) = -2c_6 + c_3$ linear functions, with $c_1, \ldots, c_6 \in \mathbb{R}$. Thus, the general solution of the determining equations is given by

$$\xi = c_1 + c_4 x + 2c_5 t + 4c_6 x t \tag{51}$$

$$\tau = c_2 + 2c_4t + 4c_6t^2 \tag{52}$$

$$\phi = (c_3 - c_5 x - 2c_6 t - c_6 x^2) u + \alpha(x, t)$$
(53)

where $c_1, \ldots, c_6 \in \mathbb{R}$ and $\alpha(x,t)$ is any solution of the heat equation $\alpha_t = \alpha_{xx}$. Using the usual basis in \mathbb{R}^6 , the Lie algebra is spanned by 6 vector fields

$$\mathbf{v}_{1} = \partial_{x} \qquad \mathbf{v}_{2} = \partial_{t} \qquad \mathbf{v}_{3} = u\partial_{u} \qquad \mathbf{v}_{4} = x\partial_{x} + 2t\partial_{t}$$

$$\mathbf{v}_{5} = 2t\partial_{x} - xu\partial_{u} \qquad \mathbf{v}_{6} = 4xt\partial_{x} + 4t^{2}\partial_{t} - (x^{2} + 2t)u\partial_{u}$$
(54)

and the subalgebra $\mathbf{v}_{\alpha} = \alpha(x,t)\partial_{u}$.

Hence, by theorem A.1 we can determine the infinitesimal generators of the symmetry group. In a next step, we have to relate these generators in the Lie algebra to the group elements. This connection is provided by the *exponential map* $\exp : \mathfrak{g} \to G$, whose action on an element $(x, u) \in M \subseteq X \times \mathcal{U}$ is described by

$$\exp(\vartheta \mathbf{v}) \circ (x, u) = \sum_{k > 0} \frac{\vartheta^k}{k!} \mathbf{v}^k \circ (x, u) . \tag{55}$$

 \triangle

Let us illustrate the application of the exponential map by continuing the previous example.

Example A.3 [Continuation of example A.2]: To compute the one-parameter group G_1 associated to the generator \mathbf{v}_1 from (54) we have to apply \mathbf{v}_1 to a graph of a function, i.e., to an element

 $(x,t,u) \in M$. We get $\mathbf{v}_1 \circ (x,t,u) = \partial_x \circ (x,t,u) = (1,0,0)$ and $\mathbf{v}^k \circ (x,t,u) = (0,0,0)$ for any k > 1. Thus, the group G_1 is acting by

$$G_1: (x,t,u) \mapsto \exp(\vartheta \mathbf{v}_1) \circ (x,t,u) = (x,t,u) + (1,0,0)\vartheta = (x+\vartheta,t,u)$$
(56)

which is nothing else than a translation in the x coordinate. Analogue, we get a translation in time

$$G_2: (x, t, u) \mapsto \exp(\vartheta \mathbf{v}_2) \circ (x, t, u) = (x, t + \vartheta, u)$$
 (57)

To compute the group G_3 note, that $\mathbf{v}_3^k \circ u = u$ for all $k \in \mathbb{N}$. Hence, the generator \mathbf{v}_3 leads to a scaling invariance

$$G_3: (x, t, u) \mapsto \exp(\vartheta \mathbf{v}_3) \circ (x, t, u) = \left(x, t, u \sum_{k>0} \frac{\vartheta^k}{k!}\right) = (x, t, e^{\vartheta}u) . \tag{58}$$

Quite similar is the computation for \mathbf{v}_4 , and with $\mathbf{v}_4^k \circ x = x$ and $\mathbf{v}_4^k \circ t = 2^k t$ we obtain

$$G_4: (x, t, u) \mapsto \exp(\vartheta \mathbf{v}_4) \circ (x, t, u) = (e^{\vartheta} x, e^{2\vartheta} t, u)$$
 (59)

To compute the group action of G_5 , note that

$$\mathbf{v}_5^k \circ u = u \sum_{0 \le m \le k/2} \frac{k!}{m!(k-2m)!} (-x)^{k-2m} (-t)^m , \qquad (60)$$

which can be shown by induction including a distinction between even and odd k. Including that relation in the series of (55) we obtain

$$G_5: (x, t, u) \mapsto \exp(\vartheta \mathbf{v}_5) \circ (x, t, u) = (x + 2\vartheta t, t, ue^{-\vartheta x - \vartheta^2 t}) . \tag{61}$$

To find the action of the group G_6 , we will use another useful property of the exponential map, which is

$$A \circ \exp(B) \circ A^{-1} = \exp(A \circ B \circ A^{-1}) \tag{62}$$

for any functions A, B with appropriate domains and codomains and where $A \circ A^{-1} = \mathbf{1}$. This relation can directly be shown by the definition (55). In particular, the so-called inversion map

$$I(x,t) = \left(\frac{x}{t^2 - x^2}, \frac{t}{t^2 - x^2}\right) \tag{63}$$

has the property $I \circ I = 1$. As we can write $\exp(\vartheta \mathbf{v}_6) = I \circ \exp(-\vartheta \partial_x) \circ I$ we will find

$$G_6: (x, t, u) \mapsto \exp(\vartheta \mathbf{v}_6) \circ (x, t, u) = \left(\frac{x}{1 - 4\vartheta t}, \frac{t}{1 - 4\vartheta t}, u\sqrt{1 - 4\vartheta t} \ e^{-\frac{\vartheta x^2}{1 - 4\vartheta t}}\right) . \tag{64}$$

The last generator \mathbf{v}_{α} will result in the action

$$G_{\alpha}: (x, t, u) \mapsto (x, t, u + \vartheta \alpha(x, t))$$
 (65)

 \triangle

In summary, we have now determined the group actions on the graph of a function $\Gamma_f \subset X \times \mathcal{U}$, i.e., the action on every point (x,u) of that graph. In a final step, we would like to transfer this action onto the function itself. For simplicity, we will focus on the case where the action of the group element $g \in G$ takes the form $(\tilde{x},\tilde{u}) = g \circ (x,u) = (\Xi_g(x),\Phi_g(x,u))$, i.e., that the action of g on x will not depend on u. For the general case, we refer to [31, sec. 2.2]. In this particular case, we have $x = \Xi_g(\tilde{x})^{-1} = \Xi_{g^{-1}}(\tilde{x})$, and therefore

$$\tilde{f}(\tilde{x}) = \Phi_g(\Xi_{q^{-1}}(\tilde{x}), f(\Xi_{q^{-1}}(\tilde{x})))$$
 (66)

Example A.4 [Continuation of example A.3]: By using (66), we can relate the group actions from example A.3 to transformations of functions. For example, for G_1 we have $\Xi_{g_{1,\vartheta}}(x) = x + \vartheta$ and $\Phi_{g_{1,\vartheta}}(x,u) = u$. With $\Xi_{g_{1,\vartheta}^{-1}}(x) = \Xi_{g_{1,-\vartheta}}(x) = x - \vartheta$, we get the transformation

$$T_{\vartheta}^{1}: f(x,t) \mapsto f(x-\vartheta,t) \tag{67}$$

as expected. By applying (66) to the other groups $G_2, \ldots, G_6, G_\alpha$, we obtain the results presented in example 2.2.

Thus, we have a framework that, in principle, allows us to compute a symmetry group for any PDE system. For PDE systems with a certain additional property, we can give even a stronger statement. According to [31, Def. 2.70], a system of PDEs \mathcal{D} is called *local solvable* at a point $(x_0, u_0^{(d)}) \in X \times \mathcal{U}^{(d)}$, if there is a smooth solution u = f(x) for x in a neighbourhood of x_0 , with $u_0^{(d)} = \operatorname{pr}^{(d)} f(x_0)$. The whole PDE system \mathcal{D} is called locally solvable, if this property holds for any point $(x_0, u_0^{(d)})$ satisfying $\mathcal{D}(x_0, u_0^{(d)}) = 0$. For a locally solvable system, we can give a sufficient and necessary description of symmetry groups:

Theorem A.5 [Infinitesimal criterion, see [31, thm. 2.71]]: Let \mathcal{D} be a locally solvable system of PDEs with maximal rank defined over $M \subseteq X \times U$ and let G be a local group of transformations acting on M. G is a symmetry group of \mathcal{D} , if and only if

$$\operatorname{pr}^{(d)} \mathbf{v}[\mathcal{D}(x, u^{(d)})] = 0, \qquad \text{whenever } \mathcal{D}(x, u^{(d)}) = 0$$
(68)

holds for any infinitesimal generator \mathbf{v} of G.

Thus, for locally solvable systems, we can derive *all* symmetry groups of the PDE system with the aforementioned framework. We would like to conclude this section by recapping all the steps to compute the symmetry group:

- 0. Check maximal rank and local solvability of \mathcal{D} .
- 1. Write an ansatz for a vector field \mathbf{v} on $X \times \mathcal{U}$ according to (42) and compute its prolongation equations (43) to (45).
- 2. Derive the infinitesimal criterion theorems A.1 and A.5, i.e., the prolongation of **v** applied on the PDE should vanish whenever the PDE is satisfied.
- 3. By comparing the coefficients of the infinitesimal criterion, one obtains an overdetermined system of simple PDEs ("determining equations").
- 4. Solve the determining equations by elementary methods, to get the most general generators \mathbf{v} and choose a basis of the subspace generated by \mathbf{v} .

- 5. Derive 1-parameter Lie groups from infinitesimal generators by the exponential map $g_{\vartheta} \circ (x,u) = \exp(\vartheta \mathbf{v}) \circ (x,u)$.
- 6. Derive the transformation maps from these group actions by (66).

There are several implementations available, which will solve this task step by step. We refer to [6, 7, 14, 36], which giving an overview about different available implementations.

References

- [1] T. Akhound-Sadegh, L. Perreault-Levasseur, J. Brandstetter, M. Welling, and S. Ravanbakhsh. "Lie Point Symmetry and Physics-Informed Networks". In: *Advances in Neural Information Processing Systems* 36 (2023), pp. 42468–42481. arXiv: 2311.04293.
- [2] G. W. Bluman, A. F. Cheviakov, and S. C. Anco. Applications of symmetry methods to partial differential equations. Applied mathematical sciences. New York, NY: Springer, 2010.
- [3] G. W. Bluman and S. Kumei. *Symmetries and differential equations*. Applied Mathematical Sciences. Berlin, Germany: Springer, 1989.
- [4] W. E. Boyce. Elementary differential equations and boundary value problems, eleventh edition loose-leaf print companion. 11th ed. Nashville, TN: John Wiley & Sons, 2016.
- [5] J. Brandstetter, M. Welling, and D. E. Worrall. "Lie Point Symmetry Data Augmentation for Neural PDE Solvers". In: Proceedings of the 39th International Conference on Machine Learning. International Conference on Machine Learning. PMLR, 2022, pp. 2241–2256.
- [6] J. Butcher, J. Carminati, and K. Vu. "A comparative study of some computer algebra packages which determine the Lie point symmetries of differential equations". In: *Computer Physics Communications* 155.2 (2003), pp. 92–114. DOI: https://doi.org/10.1016/S0010-4655(03)00348-5.
- [7] B. Champagne, W. Hereman, and P. Winternitz. "The computer calculation of Lie point symmetries of large systems of differential equations". In: Computer Physics Communications 66.2 (1991), pp. 319–340. DOI: https://doi.org/10.1016/0010-4655(91)90080-5.
- [8] T. Cohen and M. Welling. "Group equivariant convolutional networks". In: International Conference on Machine Learning. PMLR. 2016, pp. 2990–2999.
- [9] M. Cranmer, S. Greydanus, S. Hoyer, P. Battaglia, D. Spergel, and S. Ho. "Lagrangian neural networks". In: *International Conference on Learning Representations*. 2020.
- [10] J. J. Duistermaat and J. A. C. Kolk. Lie groups. Berlin, Germany: Springer, 1999.
- [11] L. C. Evans. *Partial Differential Equations*. 2nd. Vol. 19. Graduate Studies in Mathematics. American Mathematical Society, 2010.
- [12] G. H. Golub and V. Pereyra. "The differentiation of pseudo-inverses and nonlinear least squares problems whose variables separate". In: SIAM Journal on numerical analysis 10.2 (1973), pp. 413–432.
- [13] S. Greydanus, M. Dzamba, and D. Yosinski. "Hamiltonian neural networks". In: Advances in Neural Information Processing Systems. Vol. 32, 2019.
- [14] W. Hereman. "Symbolic Software for Lie Symmetry Analysis". In: CRC Handbook of Lie Group Analysis of Differential Equations. Ed. by N. Ibragimov. Vol. III. CRC Press, 1996, pp. 367–413.
- [15] A. D. Jagtap, E. Kharazmi, and G. E. Karniadakis. "Extended physics-informed neural networks (XPINNs): A generalized space-time domain decomposition based deep learning framework for nonlinear partial differential equations". In: Communications in Computational Physics 28.5 (2020), pp. 2002–2041.
- [16] F. John. Partial Differential Equations. Applied mathematical sciences. New York, NY: Springer US, 1978.
- [17] G. E. Karniadakis, I. G. Kevrekidis, L. Lu, P. Perdikaris, S. Wang, and L. Yang. "Physics-informed machine learning". In: *Nature Reviews Physics* 3.6 (2021), pp. 422–440. DOI: 10.1038/s42254-021-00314-5.
- [18] A. S. Krishnapriyan, A. Gholami, S. Zhe, R. M. Kirby, and M. W. Mahoney. "Characterizing possible failure modes in physics-informed neural networks". In: (2021). arXiv: 2109.01050.

- [19] I. E. Lagaris, A. Likas, and D. I. Fotiadis. "Artificial Neural Networks for Solving Ordinary and Partial Differential Equations". In: *IEEE Transactions on Neural Networks* 9.5 (1998), pp. 987–1000. DOI: 10.1109/72.712178. arXiv: physics/9705023.
- [20] G. K. R. Lau, A. Hemachandra, S.-K. Ng, and B. K. H. Low. "PINNACLE: PINN Adaptive ColLocation and Experimental Points Selection". In: The Twelfth International Conference on Learning Representations. 2023.
- [21] R. J. LeVeque. Finite Difference Methods for Ordinary and Partial Differential Equations: Steady-State and Time-Dependent Problems. Philadelphia, PA: Society for Industrial and Applied Mathematics, 2007. DOI: 10.1137/1.9780898717839.
- [22] L. Lu, R. Pestourie, W. Yao, Z. Wang, F. Verdugo, and S. G. Johnson. "Physics-informed neural networks with hard constraints for inverse design". In: (2021). arXiv: 2102.04626.
- [23] X. Meng, Z. Li, and G. E. Karniadakis. "PPINNs: Physics-informed neural networks with prior". In: *Journal of Computational Physics* 401 (2020), p. 109020.
- [24] G. Mialon, Q. Garrido, H. Lawrence, D. Rehman, Y. LeCun, and B. Kiani. "Self-Supervised Learning with Lie Symmetries for Partial Differential Equations". In: Advances in Neural Information Processing Systems 36 (2023), pp. 28973–29004.
- [25] J. R. Naujoks et al. Leveraging Influence Functions for Resampling Data in Physics-Informed Neural Networks. 2025. DOI: 10.48550/arXiv.2506.16443. arXiv: cs/2506.16443. Prepublished.
- [26] D. P. O'Leary and B. W. Rust. "Variable projection for nonlinear least squares problems".
 In: Computational Optimization and Applications 54.3 (2013), pp. 579–593.
- [27] F. Oliveri. "Lie Symmetries of Differential Equations: Classical Results and Recent Contributions". In: Symmetry 2.2 (2010), pp. 658–706. DOI: 10.3390/sym2020658.
- [28] F. Oliveri. "ReLie: a Reduce program for Lie group analysis of differential equations". In: (2021). arXiv: 2105.11534.
- [29] P. J. Olver. *Introduction to partial differential equations*. en. 1st ed. Undergraduate texts in mathematics. Cham, Switzerland: Springer International Publishing, 2013.
- [30] P. J. Olver. "Symmetry and explicit solutions of partial differential equations". In: Applied Numerical Mathematics 10.3 (1992), pp. 307–324. DOI: https://doi.org/10.1016/0168-9274(92)90047-H.
- [31] P. J. Olver. Applications of Lie Groups to Differential Equations. 2nd. New York: Springer-Verlag, 1993.
- [32] M. Raissi, P. Perdikaris, and G. E. Karniadakis. "Physics-informed neural networks: A deep learning framework for solving forward and inverse problems involving nonlinear partial differential equations". In: *Journal of Computational Physics* 378 (2019), pp. 686–707. DOI: 10.1016/j.jcp.2018.10.045.
- [33] P. Rathore, W. Lei, Z. Frangella, L. Lu, and M. Udell. "Challenges in Training PINNs: A Loss Landscape Perspective". In: Proceedings of the 41st International Conference on Machine Learning. Ed. by R. Salakhutdinov, Z. Kolter, K. Heller, A. Weller, N. Oliver, J. Scarlett, and F. Berkenkamp. Vol. 235. Proceedings of Machine Learning Research. PMLR, 2024, pp. 42159– 42101
- [34] J. Rauch. *Partial Differential Equations*. en. Graduate Texts in Mathematics. New York, NY: Springer, 1991.
- [35] J. Sirignano and K. Spiliopoulos. "DGM: A deep learning algorithm for solving partial differential equations". In: *Journal of Computational Physics* 375 (2018), pp. 1339–1364. DOI: 10.1016/j.jcp.2018.08.029. eprint: 1708.07469.

- [36] S. Steinberg and R. de Melo Marinho Junior. "Practical Guide to the Symbolic Computation of Symmetries of Differential Equations". In: (2014). arXiv: 1409.8364.
- [37] N. Thomas, T. Smidt, S. Kearnes, L. Yang, L. Li, K. Kohlhoff, and P. Riley. "Tensor field networks: Rotation- and translation-equivariant neural networks for 3D point clouds". In: *Advances in Neural Information Processing Systems*. Vol. 31, 2018.
- [38] I. G. Tsoulos and I. E. Lagaris. "Solving Differential Equations with Genetic Programming". In: Genetic Programming and Evolvable Machines 7.1 (2006), pp. 33–54. DOI: 10.1007/s10710-006-7009-y.
- [39] S. Wang, A. K. Bhartari, B. Li, and P. Perdikaris. "Gradient Alignment in Physics-informed Neural Networks: A Second-Order Optimization Perspective". In: (2025). arXiv: 2502.00604.
- [40] S. Wang, S. Sankaran, H. Wang, and P. Perdikaris. "An Expert's Guide to Training Physics-informed Neural Networks". In: (2023). arXiv: 2308.08468.
- [41] S. Wang, Y. Teng, and P. Perdikaris. "Understanding and Mitigating Gradient Flow Pathologies in Physics-Informed Neural Networks". In: SIAM Journal on Scientific Computing 43.5 (2021), A3055–A3081. DOI: 10.1137/20M1318043.
- [42] S. Wang, Y. Teng, and P. Perdikaris. "When and why PINNs fail to train: A neural tangent kernel perspective". In: Journal of Computational Physics 449 (2022), p. 110768.
- [43] E. P. Wigner. Symmetries and reflections: scientific essays. Indiana University Press, 1967.
- [44] C. Wu, M. Zhu, Q. Tan, Y. Kartha, and L. Lu. "A Comprehensive Study of Non-Adaptive and Residual-Based Adaptive Sampling for Physics-Informed Neural Networks". In: Computer Methods in Applied Mechanics and Engineering 403 (2023), p. 115671. DOI: 10.1016/j.cma. 2022.115671.
- [45] J. Yang, N. Dehmamy, R. Walters, and R. Yu. "Latent Space Symmetry Discovery". In: *Proceedings of the 41st International Conference on Machine Learning*. Vol. 235. ICML'24. Vienna, Austria: JMLR.org, 2024, pp. 56047–56070.
- [46] J. Yang, W. Rao, N. Dehmamy, R. Walters, and R. Yu. "Symmetry-Informed Governing Equation Discovery". In: Advances in Neural Information Processing Systems 37 (2024), pp. 65297–65327.
- [47] Z.-Y. Zhang, S.-J. Cai, and H. Zhang. "A Symmetry Group Based Supervised Learning Method for Solving Partial Differential Equations". In: Computer Methods in Applied Mechanics and Engineering 414 (2023), p. 116181. DOI: 10.1016/j.cma.2023.116181.
- [48] Z.-Y. Zhang, H. Zhang, L.-S. Zhang, and L.-L. Guo. "Enforcing continuous symmetries in physics-informed neural network for solving forward and inverse problems of partial differential equations". In: *Journal of Computational Physics* 492 (2023), p. 124145.